

AD-A009 284

STUDIES OF E-BEAM PUMPED MOLECULAR
LASERS

D. L. Huestis, et al

Stanford Research Institute
Menlo Park, California

31 January 1975

DISTRIBUTED BY:

NTIS

National Technical Information Service
U. S. DEPARTMENT OF COMMERCE

ACCESSION for	
NTIS	White Section <input checked="" type="checkbox"/>
DDC	Buff Section <input type="checkbox"/>
UNANNOUNCED	<input type="checkbox"/>
JUSTIFICATION.....	
BY.....	
DISTRIBUTION/AVAILABILITY CODES	
Dist.	Avail. and/or SPECIAL
A	

The views and conclusions contained in this document are those of the authors and should not be interpreted as necessarily representing the official policies, either expressed or implied, of the Advanced Research Projects Agency of the U.S. Government.

id

UNCLASSIFIED

SECURITY CLASSIFICATION OF THIS PAGE (When Data Entered)

REPORT DOCUMENTATION PAGE		READ INSTRUCTIONS BEFORE COMPLETING FORM	
1. REPORT NUMBER	2. GOVT ACCESSION NO.	3. RECIPIENT'S CATALOG NUMBER AD-A009 284	
4. TITLE (and Subtitle) STUDIES OF E-BEAM PUMPED MOLECULAR LASERS		5. TYPE OF REPORT & PERIOD COVERED Technical Report No. 4 1 July 1974 to 31 December 1974.	
7. AUTHOR(s) D. L. Huestis, R. A. Gutcheck, R. M. Hill, M. V. McCusker, and D. C. Lorents		6. PERFORMING ORG. REPORT NUMBER MP 75-18	
9. PERFORMING ORGANIZATION NAME AND ADDRESS Stanford Research Institute 333 Ravenswood Avenue Menlo Park, California 94025		10. PROGRAM ELEMENT, PROJECT, TASK AREA & WORK UNIT NUMBERS	
11. CONTROLLING OFFICE NAME AND ADDRESS Advanced Research Projects Agency 1400 Wilson Boulevard Arlington, Virginia 22209		12. REPORT DATE 31 January 1975	13. NO. OF PAGES 90
14. MONITORING AGENCY NAME & ADDRESS (if diff. from Controlling Office) Office of Naval Research 800 N. Quincy Street Arlington, Virginia 22217		15. SECURITY CLASS. (of this report) UNCLASSIFIED	
16. DISTRIBUTION STATEMENT (of this report) Distribution of this document is unlimited.		15a. DECLASSIFICATION/DOWNGRADING SCHEDULE	
17. DISTRIBUTION STATEMENT (of the abstract entered in Block 20, if different from report)		<div style="text-align: center;"> DDC RECEIVED MAY 12 1975 REGULATED D </div>	
18. SUPPLEMENTARY NOTES		Reproduced by NATIONAL TECHNICAL INFORMATION SERVICE US Department of Commerce Springfield, VA. 22151	
19. KEY WORDS (Continue on reverse side if necessary and identify by block number)			
Electron beam	Xenon	O(¹ S)	Potential curves
Molecular laser	Oxygen	XeO	Reaction kinetics
Energy transfer	Rare gas oxides		
Rare gas dimers	Excimers		
PRICES SUBJECT TO CHANGE			
20. ABSTRACT (Continue on reverse side if necessary and identify by block number)			
This report summarizes our continued studies of prospective high-power high-efficiency laser media. Included here are the results of a spectroscopic survey of light emission arising from a variety of atomic and molecular gases contained in electron-beam excited rare gas hosts. Also, to predict a laser behavior, a detailed kinetic model is developed for the xenon-oxygen system, one of the most promising candidates in the survey. To allow the development of this model, several rate constants were measured for the first time. In addition, the			

DD FORM 1473
1 JAN 73
EDITION OF 1 NOV 65 IS OBSOLETE

UNCLASSIFIED

SECURITY CLASSIFICATION OF THIS PAGE (When Data Entered)

UNCLASSIFIED

SECURITY CLASSIFICATION OF THIS PAGE (When Data Entered)

19. KEY WORDS (Continued)

20 ABSTRACT (Continued)

structures of several xenon oxide levels were determined from spectroscopic observations. The kinetic model suggests that a xenon oxide laser may operate with an efficiency as high as 6% for the 537.6 nm band and as high as 11% at 308.0 nm.

ia

UNCLASSIFIED

SECURITY CLASSIFICATION OF THIS PAGE (When Data Entered)

CONTENTS

ILLUSTRATIONS	ii
TABLES	iv
SUMMARY	1
BACKGROUND	3
INTRODUCTION TO XENON OXIDE	5
EXPERIMENTAL APPARATUS AND PROCEDURE	7
THE ENERGY LEVELS AND SPECTRUM OF XeO	11
The Major Green Bands ($\lambda\lambda 4800-5600 \text{ \AA}$): $2^1\Sigma^+ \rightarrow 1^1\Sigma^+ \dots$	14
The Minor Green Bands ($\lambda\lambda 5600-5800 \text{ \AA}$): $2^1\Sigma^+ \rightarrow 1^1\Pi \dots$	19
The UV Continuum ($\lambda 3080 \pm 40 \text{ \AA}$): $2^1\Sigma^+ \rightarrow 1^3\Pi \dots$	19
The Potential Curves for XeO.....	25
PRODUCTION OF O(1S) IN XENON-OXYGEN MIXTURES	30
Quenching of Xe ₂ [*]	32
Ozone Formation	39
THE DECAY OF XeO	43
THE KINETIC MODEL	51
Quenching by O(3P)	56
Production of O(1S)	60
LASER OPERATION	64
CONCLUSIONS	69
REFERENCES	70
APPENDIX: Optical Emissions from e-Beam Excited Gas Mixtures	A1

ILLUSTRATIONS

1. Schematic diagram of apparatus.....	8
2. Energy levels of the $2p^4$ configuration of atomic oxygen.....	12
3. Green and ultraviolet emission bands of XeO.....	15
4. Densitometer trace of XeO green band emissions.....	16
5. Vibrational spacings for the low-lying bound Singlet states of XeO.....	18
6. Photographic display of the minor green bands of XeO.....	20
7. Densitometer trace of the XeO minor green band system.....	21
8. Densitometer trace of XeO uv continuum.....	24
9. Morse potentials for the low-lying bound Singlet states of XeO.....	26
10. Semiquantitative potential curves for the low-lying states of XeO.....	28
11. Selected energy levels for Xe, O_2 , O, CO_2 , N_2O , O_3	31
12. Schematic potential curves for energy transfer from Xe_2^* to $O(^3P)$	33
13. Pressure dependence of xenon excimer radiative decay frequency (10^2 - 10^5 torr).....	34
14. Pressure dependence of xenon excimer radiative decay frequency (0-4000 torr).....	36
15. Xenon pressure dependence of time-integrated excimer emission.....	37
16. Oxygen quenching of xenon excimer fluorescence.....	38
17. Ozone production in Febetron excited xenon/oxygen mixtures.....	41

18. Oxygen pressure dependence of XeO decay.....	46
19. Xenon pressure dependence of XeO decay.....	47
20. Oxygen pressure dependence of XeO fluorescence intensity compared with preliminary kinetic model.....	48
21. Xenon pressure dependence of XeO fluorescence intensity compared with preliminary kinetic model.....	49
22. Energy flow in Xenon/oxygen mixtures.....	53
23. Quenching of $O(^1S)$, and indirectly XeO, by $O(^3P)$	58
24. Quenching of Xe_2^* by $O(^3P)$	59
25. Linear plot of $O(^1S)$ versus O_2Z^2	61
26. Logarithmic plot of $O(^1S)$ versus O_2Z^2	62
27. $O(^1S)$ number efficiency versus xenon pressure.....	67

TABLES

I	$2^1\Sigma^+ \rightarrow 1^1\Pi$ Bands of XeO	22
II	Delandres Table for the $2^1\Sigma^+ \rightarrow 1^1\Pi$ Bands of XeO	23
III	Spectroscopic Constants for the Singlet States of XeO ...	29
IV	Rate Coefficients for Collision-Induced Emission of $O(^1S)$ by Xe	45
V	Reactions in Xenon/Oxygen Mixtures	63

SUMMARY

The purpose of this program is to develop an understanding of the molecular kinetics pertinent to new high efficiency, high power electronic transition lasers. We are studying high pressure gases that are initially excited by intense bursts of electrons. This initial pumping energy, which is primarily deposited by creating atomic ions, rapidly collects in the lowest molecular excited state with an overall efficiency for the rare gases near 50%.

Rare gas dimers for which the ground level is repulsive, in particular Xe_2 , Kr_2 , and Ar_2 , have already demonstrated laser action but with disappointing efficiencies. This problem, coupled with the relatively high gain (implying low energy storage capacity) and with vacuum ultraviolet wavelength, has led us to consider ways of transferring the energy deposited in the rare gas to other gas molecules to improve total efficiency, shift the wavelength to the near ultraviolet or visible, and improve the energy storage capacity.

In this report we describe generally our experimental survey of candidate gas mixtures and our detailed studies of the $\text{Xe} + \text{O}_2$ system.

The important results in summary are:

(1) Energy from a high energy electron beam can be efficiently transferred into excited states of the rare gases and then transferred to specific excited states of other gases.

(2) The weakly bound excimer $\text{XeO}(2^1\Sigma^+)$, which is formed from $\text{Xe} + \text{O}(^1\text{S})$, is an excellent laser candidate with possible efficiencies of 6% and 11% in the green (5376\AA) and uv (3080\AA) bands respectively.

(3) From our kinetic studies we have concluded that the efficient production of XeO proceeds through two energy transfer steps: first, dissociation of O_2 ; and second, excitation of $\text{O}(^3\text{P})$ to $\text{O}(^1\text{S})$.

(4) Kinetic modeling, coupled with experiments to determine excited state populations and reaction rate coefficients, can lead to the discovery of new laser systems and guide their development.

Measurements were made of the density of the Xe_2^+ and XeO excimers and their temporal behavior following excitation of the xenon. Estimates of the extent of O_2 dissociation were obtained from absorption measurements of the ozone produced by the recombination of the oxygen atoms. These data allowed us to determine a number of reaction rate coefficients that could be combined with others obtained from the literature to construct a preliminary kinetic model. The agreement between this model and our experimental observation supports our picture of the important energy pathways and has allowed the prediction of possible laser efficiencies.

BACKGROUND

A considerable effort has been devoted recently to the development of high energy vacuum ultraviolet lasers by pumping high pressure rare gases with electron beams (KFRE72, HSR73a-b, GJ73a-b). Efficiencies for the conversion of electrical energy into excited electronic states of the rare gases may be as high as 50% (LO72, CoC74). At high pressures this stored energy can be extracted as vuv radiation from the excited rare gas dimers (excimers). Moreover, for sufficiently rapid and intense energy deposition, lasing action has been shown to occur on the excimer transitions. Unfortunately, experimental results and more detailed models (LEH73, GR73, HSRWG74) have indicated that photoionization of the excimers and other processes limit the laser efficiency to about 1%, far less than the earlier expectations of high laser efficiencies that were based on the repulsive nature of the rare gas ground state potentials. In any event, the detailed models (LEH73, GR73, HSRWG74) and the experiments (KFRE74) clearly indicate that the excimer levels can be efficiently populated by e-beam pumping under the proper conditions.

We are seeking ways to make use of the efficient and specific energy available in the rare gas excited states to produce laser action in the visible or near uv range. Perhaps the most straightforward approach is to collisionally transfer the excitation directly to another radiating system, atom, or molecule to achieve laser action in these systems. For this approach to be ideal, the transfer rate should be rapid and specific, populating only one or two excited states of the acceptor. These states should be somewhat metastable against radiation and strongly resistant to quenching, and of course the lower level should be unpopulated and strongly quenched by either radiation or collision.

The basis of our approach has been an experimental survey of possible candidates, followed by detailed kinetic analysis of the transfer and quenching processes for favorable systems, leading to meaningful predictions of potential laser efficiencies. A preprint of a paper (which has been accepted for publication in the J. of Applied Physics) describing some preliminary results of our on-going survey program is provided as an appendix.

Our initial survey work revealed the great promise of the Ar + N₂ system. It has now been studied in considerable detail [see our preceding report (HGHML74)]. The kinetic model we developed, supported by our experimental observations, gave predictions of operating efficiencies of 1% in the near uv, 2% in the near ir, and a potential efficiency of 10-20% in several bands near 2500 Å. Observation of laser operation at NRL (SH74) and Northrop (ABO74) and recently at LASL (Hu74) have supported our efficiency estimate for the 3577 Å and 3805 Å emissions from N₂(C³Π_u). Laser action on the first-positive and Vegard-Kaplan systems remains to be demonstrated.

Our survey also indicated the promise of energy transfer from xenon to oxygen containing molecules. This report describes in detail our experimental observations and theoretical analyses to date. In our studies of the Xe + O₂ system we believe that we have identified the important energy pathways. Preliminary values for most of the necessary reaction rate coefficients have been obtained from analysis of the kinetic data. The kinetic picture is not yet complete, but it appears that efficiencies as high as 6% (at 5376⁰Å) and 11% (at 3080⁰Å) may be attainable under optimum conditions.

INTRODUCTION TO XENON OXIDE

In the search for efficient, high power lasers much attention is being paid to species that are radiatively and collisionally metastable. It is difficult to obtain a large excited state population and hence high energy density unless the spontaneous radiative and collisional decay occur on a time scale significantly longer than the available pumping rates. Of particular concern is the excited state-excited state mutual destruction rate. Further, the necessity of depopulating the lower laser level must not be ignored.

In a recent report, Murray and Rhodes (MR73) have suggested the second metastable level of the oxygen atom as satisfying the above criteria. The free radiative lifetime of $O(^1S)$ is about 0.8 sec (NSW 71, CoW72). Collisional quenching by most gases is quite slow; in particular it is generally much slower than the quenching of $O(^1D)$ (see DH70). If a sufficiently efficient production scheme can be identified, then a laser based on $O(^1S)$ could be very promising for a variety of applications.

In our survey study of laser candidates that utilize energy transfer from rare gas metastable atoms and excimers, our interest in $O(^1S)$ is somewhat accidental. We found that in Febetron excited xenon, even in the absence of intentional sources of oxygen, the green and uv bands of XeO were frequently the dominant emissions. Subsequent to our preliminary observation (GHHNL73), and in cooperation with our efforts, the Livermore group has observed (MPR74, PMR74a-b) strong laser action in XeO, KrO and ArO. We report here a summary to date of our efforts to understand the structure of the XeO molecule and the kinetic processes that govern its production and decay. A portion of this work was described at a recent conference (LHGHN74).

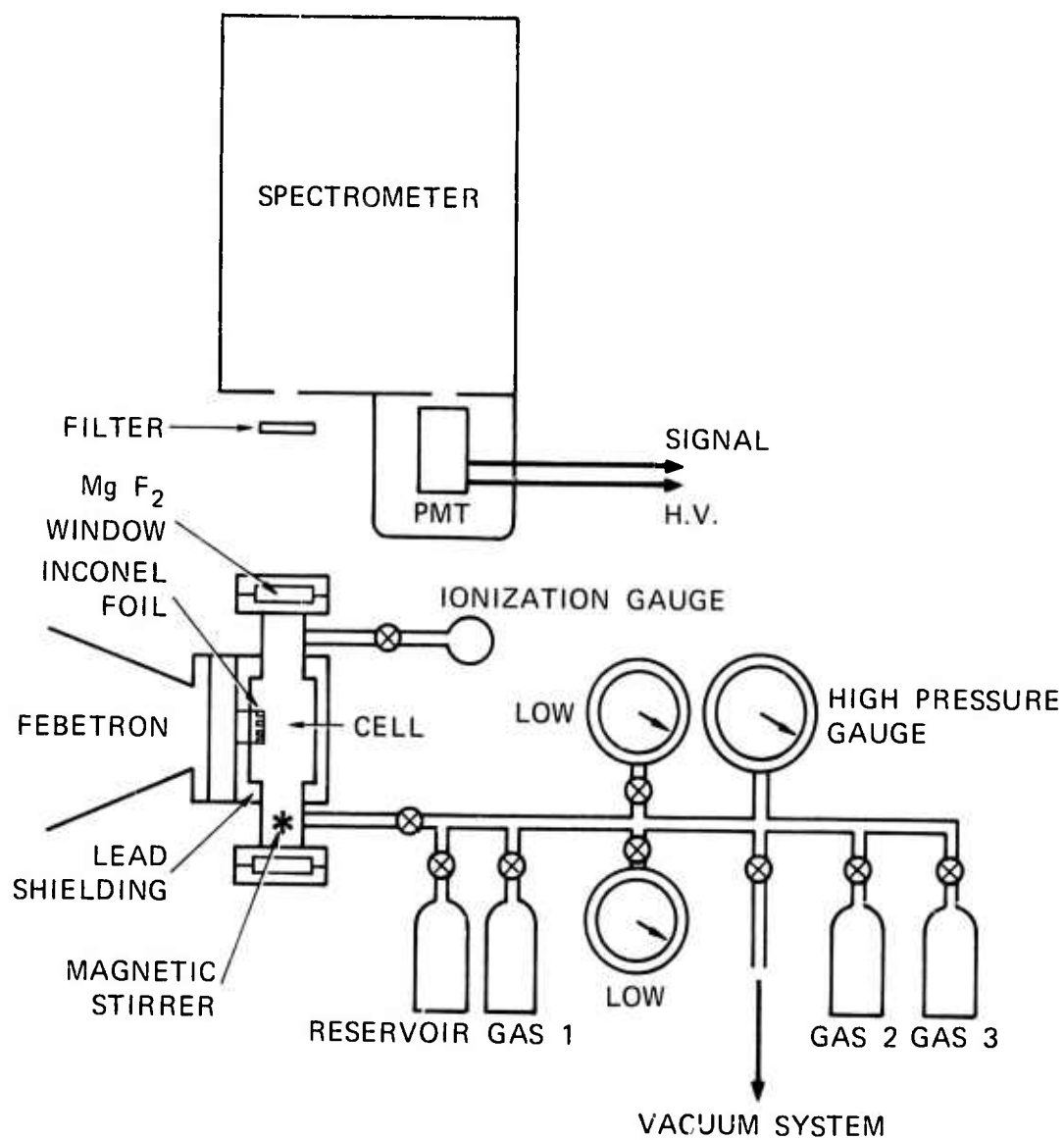
The central problem is trying to construct an adequate kinetic model is to deduce the behavior of the non-radiative species, $O(^3P)$, $O(^1S)$ and O_2 from the behavior of the directly observable species, XeO , Xe_2^* and O_3 . After a brief description of our experimental procedures, we describe the structure and spectra of the XeO molecule. Next, the steps leading to production of $O(^1S)$ atoms are detailed, and this is followed by a discussion of the time behavior of the observed XeO radiation. The kinetic model is then constructed and used to derive predictions for $O(^1S)$ production. Finally, estimates are given for possible laser efficiencies under optimum conditions.

EXPERIMENTAL APPARATUS AND PROCEDURE

The experimental system is quite similar to the one described in our previous report (HGML74) and is schematically presented in Figure 1. Optical emissions, resulting from the pulsed electron excitation of a gas mixture under high pressure, are viewed by a 0.5 meter monochromator-spectrograph (McPherson model 216.5). A Febetron 706 (Hewlett Packard) provides a 2 to 3 nsec, 6000 amp pulse of 600 KeV electrons, which enter a stainless steel experimental cell through an inconel foil (1 mil thickness). The cell has windows made of MgF_2 and is designed to operate with sample gas pressures between 200 and 10,000 torr (approximately 0.25 to 15 atmospheres). By evacuating both the spectrometer and the passage between the cell window and the spectrometer entrance slits, we have been able to view the Xe_2^* excimer radiation at 1720 \AA .

As described in some greater detail below, each Febetron shot into a xenon/oxygen mixture dissociated a significant portion of the O_2 (as much as 10%). On the second and subsequent shots the XeO signal was found to be more intense and to decay more rapidly. This is interpreted in terms of ozone formed by recombination of the dissociated oxygen. It was therefore necessary for the gas mixture to be pumped out and a new charge of gas to be added before the next excitation pulse could be delivered. We found that our magnetic stirrer enabled us to do these steps every 15 minutes. Each data point presented represents a new mixture of $\text{Xe} + \text{O}_2$ with measured number densities of O_2 and Xe .

Our time-integrated spectra of the emissions have been taken on both Kodak Tri-X (400 ASA) and Polaroid Type 57 (3000 ASA) film. Band structures and wavelengths are then determined with the aid of either a microdensitometer or a travelling microscope. The temporal behavior of



SA-1925-82R

FIGURE 1 SCHEMATIC DIAGRAM OF APPARATUS

the XeO emissions is recorded by photographing the oscilloscope traces (Tektronix model 485) of individual excitation pulses as detected by a photomultiplier (RCA 1P28).

For our time decay studies, we looked at 5376 Å (major green bands), 5650 Å (minor green bands), 3080 Å (uv bands), and 1720 Å (Xe_2^* excimer bands). The absorption studies, which monitored the growth of the O_3 density, were made by measuring the transmission through the cell of the 2537 Å emissions from a mercury pen lamp.

We found that the temporal behavior of the 5376, 5650, and 3080 Å decays was the same in terms of rise time (50-200 nsec), time of peak signal, and decay time (0.5-10 μsec). Further, the relative intensities of the various XeO emissions were found to be independent of gas pressure and composition. Most of our data was taken at 5376 Å. Spot checks of the other band systems showed identical temporal behavior. The Xe_2^* excimer vuv emission near 1720 Å was detected by depositing a layer of sodium salicylate on the PMT glass envelope. Unfortunately the natural decay time of this scintillator (9-11 nsec) prevented the monitoring of decay frequencies faster than about $7 \times 10^7 \text{ sec}^{-1}$.

The relative intensities of the green and uv emissions were determined by computing the total photon flux that was emitted by each band system, and then taking the ratio of the two fluxes. Our slit function measurements (determining how much of the total band is viewed by the band pass of our spectrometer) contributes the largest error (30%) to our ratio value. Accurate determination of the XeO uv emission intensity is complicated by the broad but fast decaying continuum background underlying the slower decaying narrow XeO band. This same superposition has been observed by Cunningham and Clark (CuC74).

Our determination of the number densities of Xe_2^* was based on an absolute calibration of the vuv spectrometer system. We were able to extend our previously computed values (from 2470 Å to the longer wavelengths)

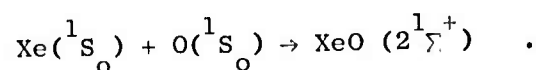
down to 1700 Å by combining the molecular branching ratio method (MuZ71) with our procedure of using a tungsten ribbon filament radiance lamp. For the branching ratio method, we used both the NO γ bands and the CO 4+ bands. We do not feel that the calibration at this time can give absolute values to better than a factor of 3.

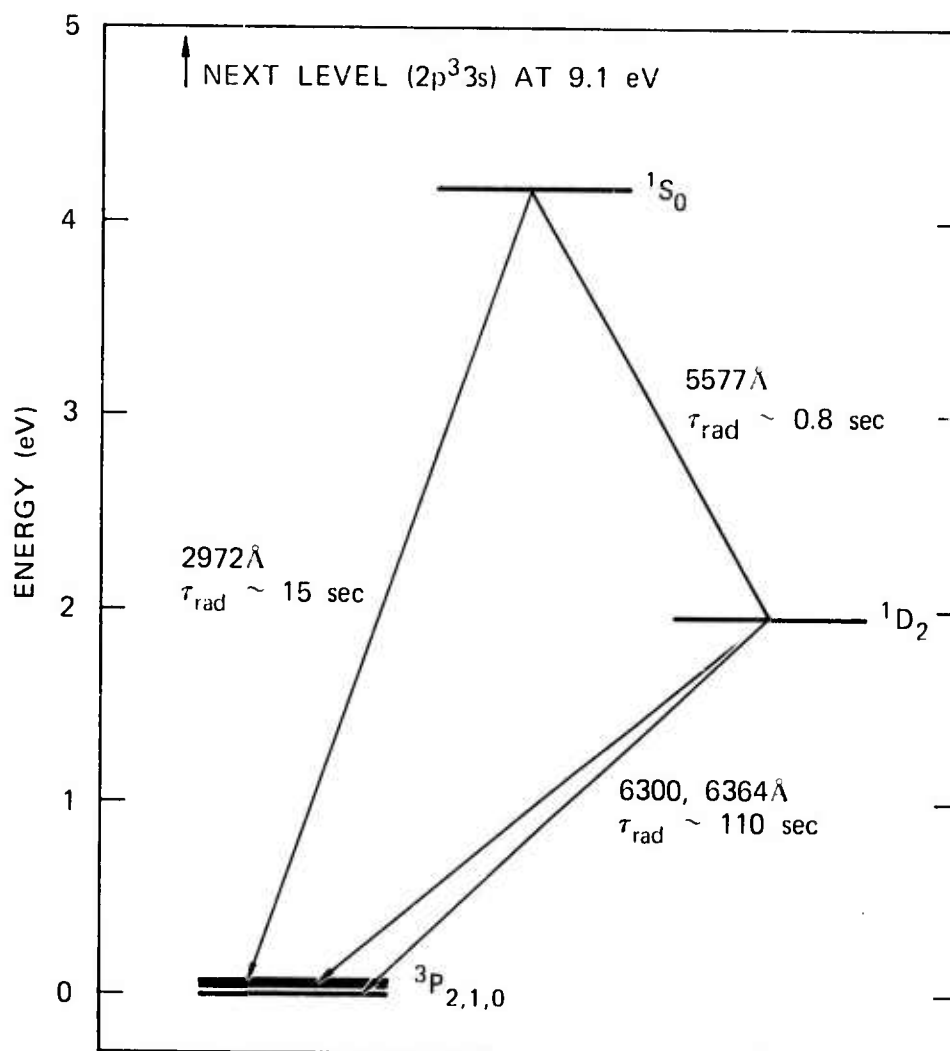
THE ENERGY LEVELS AND SPECTRUM OF XeO

The green emission bands of the XeO molecule were first reported by Kenty et al (KANPP46) from a xenon-oxygen high frequency discharge. They mention that even at the 1 ppm level of O₂ the XeO bands can be detected. A number of investigators have studied these bands in the region 4800-5800 Å (HH50, CCT61, Co?, Wi65, CuC74). Other emissions in the regions 6500-8600 Å and 2900-3200 Å have been observed as well (HH50, CCT61, CuC74). Each of these emission features may be correlated with the various forbidden transitions in the oxygen atom, but each is shifted, broadened, and intensified by formation of the weakly bound XeO molecule.

Figure 2 shows an energy diagram for the oxygen atom, with some of the transition wavelengths listed. The correspondence between atomic transitions and the green, red, and uv bands of XeO is at least suggestive and perhaps obvious. It remains then to examine in detail the spectra and potential curves that give rise to them. Our discussion here will concentrate on the green and uv bands. These are the emissions that have been studied in our laboratory, and they hold the best promise of efficient laser action.

We first describe the symmetries of the states to be expected by combination of a xenon atom and an oxygen atom. The xenon atom has a 1S_0 ground state. Its first excited state lies at 8.3 eV. Combination with O(1S) yields a single electronic state

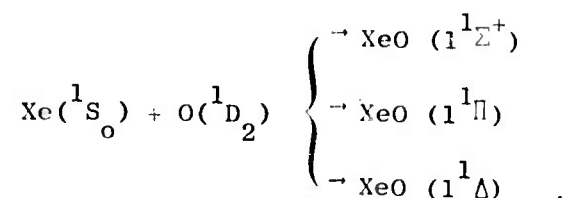




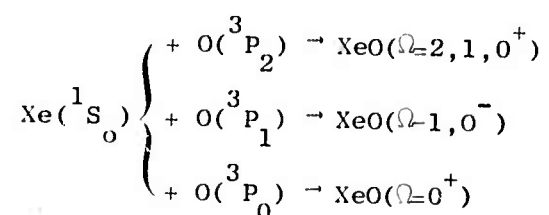
SA-1925-107R

FIGURE 2 ENERGY LEVELS OF THE $2p^4$ CONFIGURATION OF ATOMIC OXYGEN

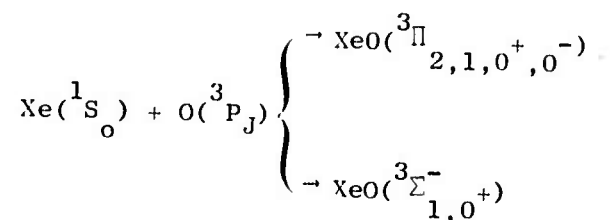
Combination with $O(^1D_2)$ yields three possible states:



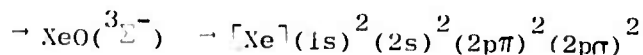
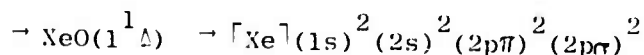
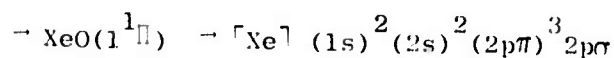
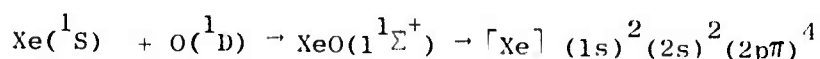
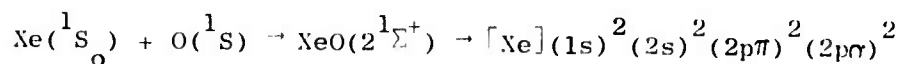
The states arising from $O(^3P)$ are slightly more complicated. At large internuclear separations (perhaps to within the van der Waals radius) the oxygen spin-orbit interaction is dominant:



At smaller internuclear distances the electrostatic repulsion overwhelms the spin-orbit interaction, then the spin and electronic angular momentum recouple to give



Examining the molecular orbital configurations in greater detail allows us to order these various states with respect to their energies. In particular we see that



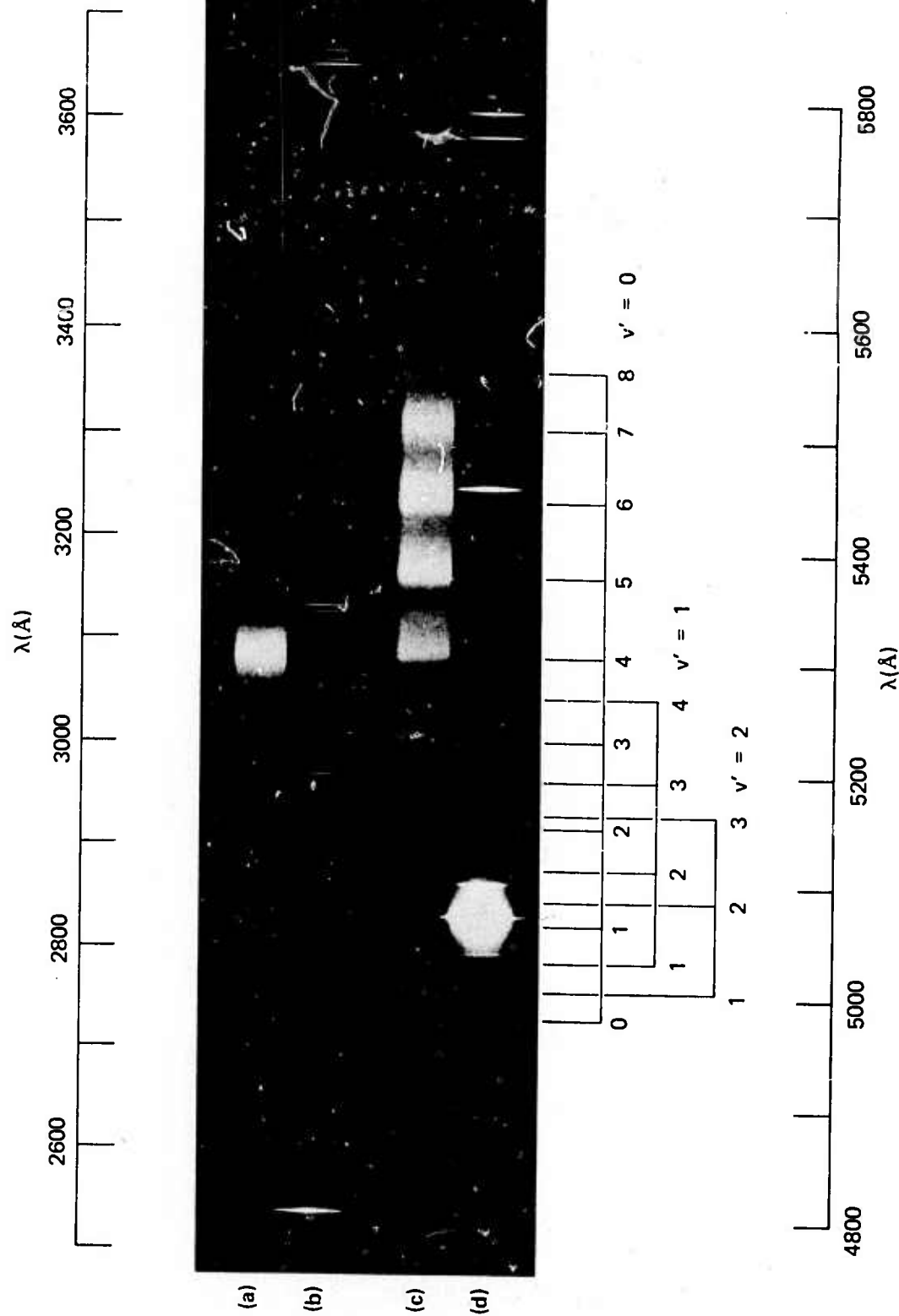
Essentially the strength of the repulsion between the oxygen and the xenon can be correlated with the number of $2p\sigma$ electrons that the oxygen atom points toward the xenon. Specifically we would expect the $^3\Sigma^-$, $^1\Delta$, and $2^1\Sigma^+$ states to be strongly repulsive, somewhat less repulsive will be the $^3\Pi$ and $^1\Pi$, finally the $1^1\Sigma^+$ is expected to be bound. In fact, the binding of the $1^1\Sigma^+$ is rather stronger than would be anticipated from these simple arguments. Much of the binding arises from partial inclusion of ionic character ($\text{Xe}^+ \text{O}^-$) into the electron distribution. It is this same ionic character that gives rise to the small attractive well in the $2^1\Sigma^+$, in spite of the repulsive nature of the simple covalent configuration above.

The Major Green Bands ($\lambda\lambda$ 4800-5600 Å): $2^1\Sigma^+ \rightarrow 1^1\Sigma^+$

The various XeO emissions we have observed are shown in Figure 3 (a low resolution, ± 1 Å, Polaroid print). The green bands are shown in greater detail in Figure 4 (a logarithmic densitometer trace). The assignment of the $2^1\Sigma^+ \rightarrow 1^1\Sigma^+$ vibrational bands is due to Cooper et al. (CCT61).^{*} To our knowledge two attempts have been made to perform a rotational analysis on this transition (CCT61, Co?, Wi65). Indeed,

* There are a number of typographical errors in this paper (CCT61). In Table I the assignment of bands 3,1 and 0,0 should be interchanged. In Table II transition 0,6 should read 18372 cm^{-1} . The entry for 4,1 was entered twice; it should read:

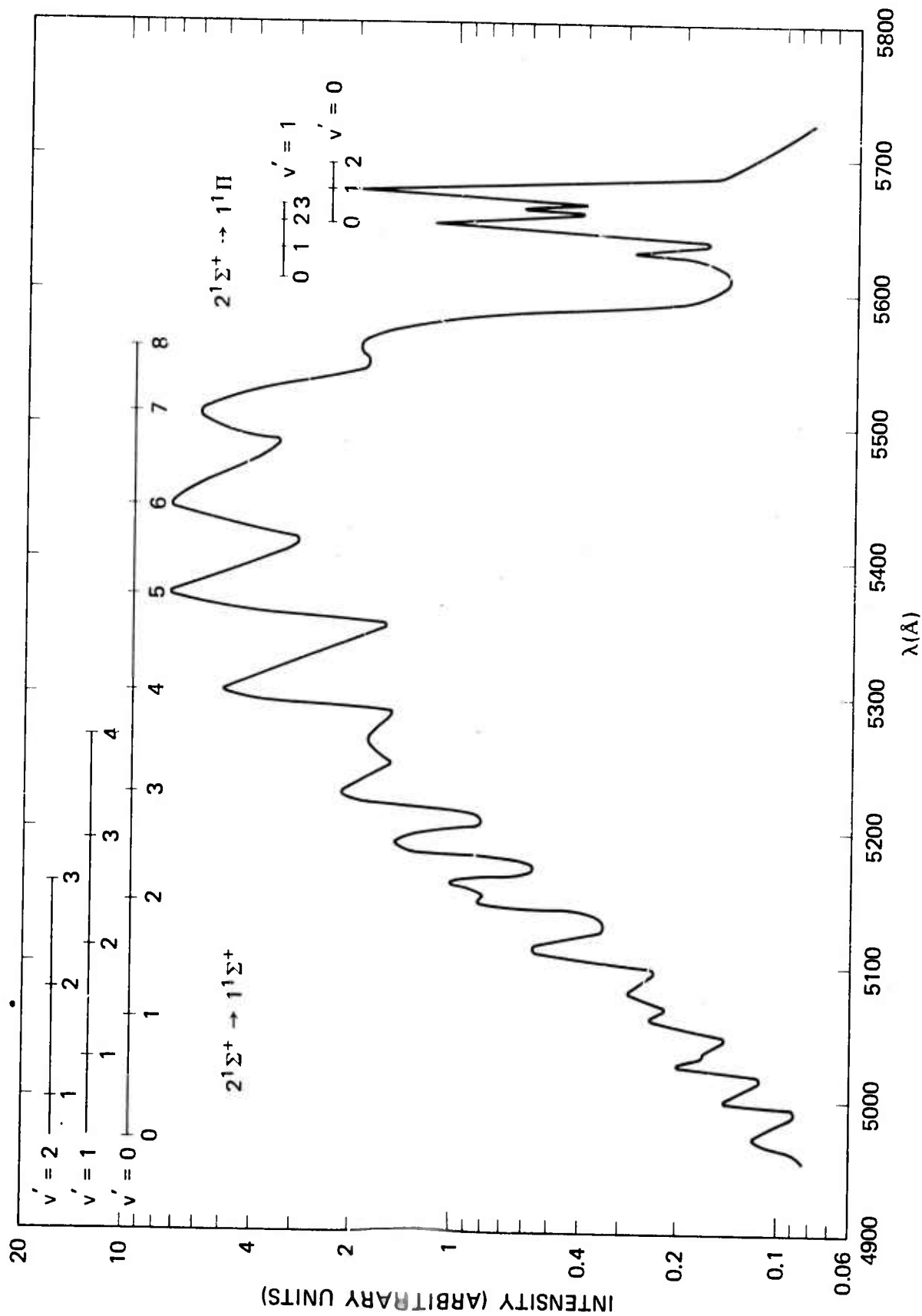
	4	5	6	7
1	20135 (56)	20219 (43)	20262 (39)	20301



SA-1925-42R1

FIGURE 3 GREEN AND ULTRAVIOLET EMISSION BANDS OF XeO

(a) uv continuum of XeO (upper scale); (b) Hg calibration lines (upper scale); (c) green band of XeO, vibrational assignments of $2^1\Sigma^+ \rightarrow 1^1\Sigma^+$ are given (lower scale); (d) Hg calibration lines (lower scale).



SA-1925-40

FIGURE 4 DENSITOMETER TRACE OF XeO GREEN BAND EMISSIONS

Cooper used the absence of a Q-branch to assign the electronic symmetries. Unfortunately a detailed analysis is immensely complicated by nearly equal abundance of the three most common isotopes of Xe, with a total of seven isotopes of 1.9% abundance or greater. This means that all the rotational lines are blurred, and for high J, badly overlapped. The inability of Cooper et al (CCT61) and Wilt (Wi65) to agree on the rotational assignments indicates a need for a careful analysis of the spectrum of isotopically pure XeO.

One would like to obtain from the spectroscopic analysis a dissociation energy for each of the various excited states. To examine the information available, a graph of $\Delta G(v)$ versus v for the $1^1\Sigma^+$ state is shown in figure 5. To obtain a value for the dissociation energy, an extrapolation to $\Delta G = 0$ is necessary, but it is a very long one, and uncertainties of at least 100 cm^{-1} must be expected. The formula we have used is $G_1(v) = 357.66v - 11.08 v^2 - 0.08 v^3 \text{ cm}^{-1}$, with $D_0(1^1\Sigma^+) = 2617 \text{ cm}^{-1}$.

The graph of $\Delta G(v)$ is also shown for the upper state, $2^1\Sigma^+$. We have used $G_0(v) = 143v - 10v^2 \text{ cm}^{-1}$. We notice a marked break in the vibrational spacings above $v'=4$. Cooper et al. used a cubic fit to represent this change in vibrational progression. We have chosen an alternative explanation, namely that the levels above $v'=4$ are actually above the dissociation limit, and radiate as transient states inside a potential barrier. This may be supported by the observation of Cooper et al that the higher v' levels in the $2^1\Sigma \rightarrow 1^1\Sigma^+$ transition do not show fine structure. Further support is obtained from the dissociation energy of the $1^1\Pi$ state to be discussed below, and by qualitative remarks above discussing the origin of the binding in the XeO ($2^1\Sigma^+$) state.

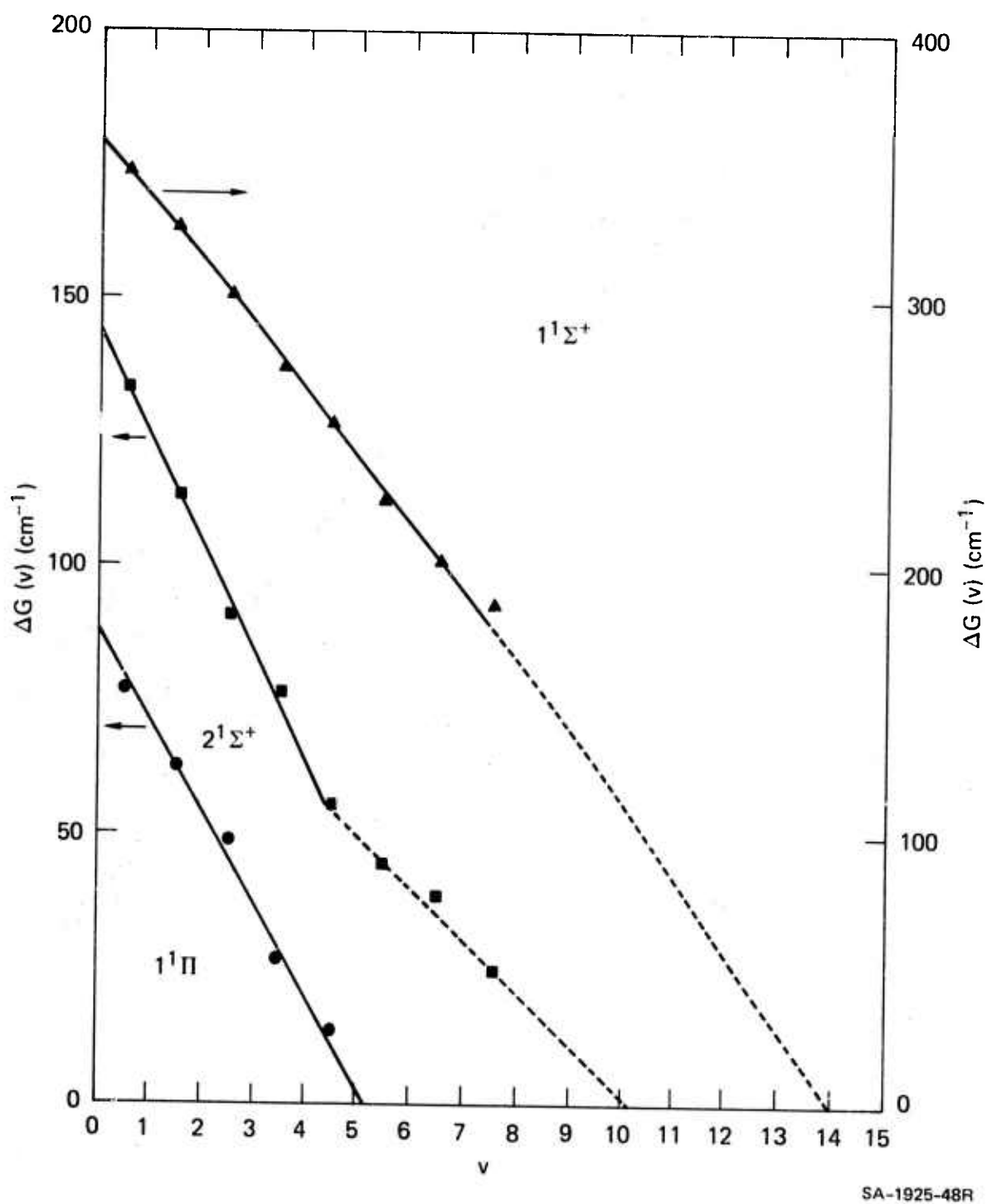


FIGURE 5 VIBRATIONAL SPACINGS FOR THE LOW-LYING BOUND SINGLET STATES OF XeO

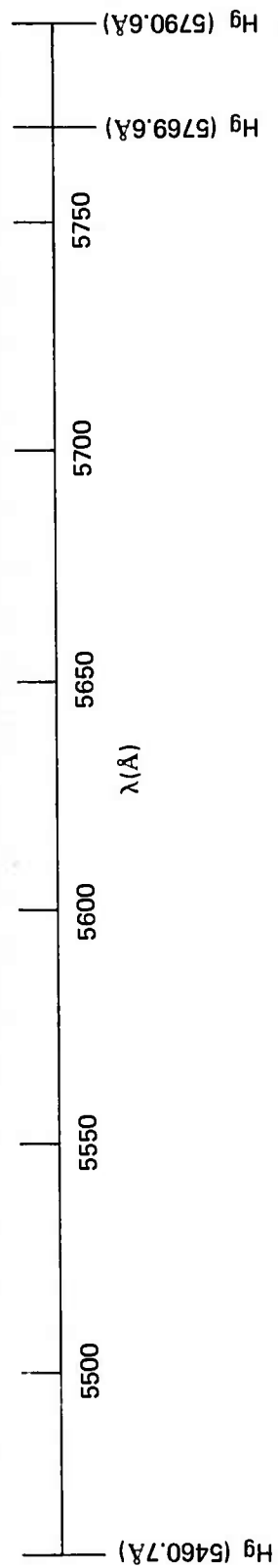
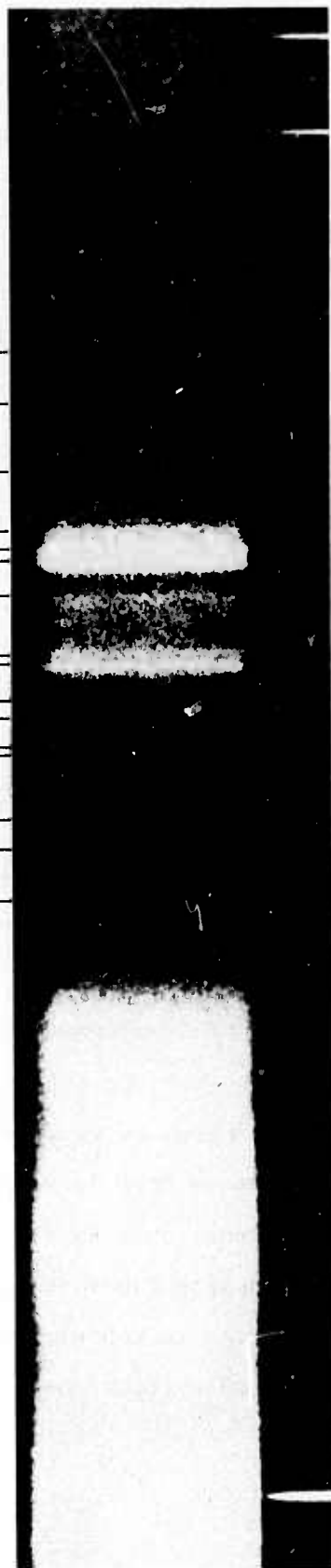
The Minor Green Bands ($\lambda\lambda 5600-5800 \text{ \AA}$), $2^1\Sigma^+ \rightarrow 1^1\Pi$:

The XeO emission bands near 5650 and 5675 \AA are shown in Figure 6 (polaroid print) and in Figure 7 (densitometer trace). These sharp but complicated features have been recorded previously (KANPP46, HH50, CCT61) but not analyzed. We have attributed these emissions to the $2^1\Sigma^+ \rightarrow 1^1\Pi$ transition. The preliminary vibrational assignments are given in Table I. Table II gives a Deslandres display of the vibrational bands. See Figure 5 for a plot of $\Delta G(v)$. The vibrational constants $\omega_e = 97 \text{ cm}^{-1}$, $\omega_e x_e = 8.7 \text{ cm}^{-1}$, yield a dissociation energy of $D_0(1^1\Pi) = 222 \text{ cm}^{-1}$. This fixes the absolute energy scale for the $2^1\Sigma^+$ and $1^1\Sigma^+$ states as well, removing the need for a long extrapolation. This yields $D(2^1\Sigma^+) = 450 \text{ cm}^{-1}$, $D_0(1^1\Sigma^+) = 2617 \text{ cm}^{-1}$ and places $v' = 5, 6, 7, 8$ of the $2^1\Sigma^+$ above the $O(^1S)$ dissociation limit.

The uv Continuum ($\lambda 3080 \pm 40 \text{ \AA}$): $2^1\Sigma \rightarrow 1^3\Pi$

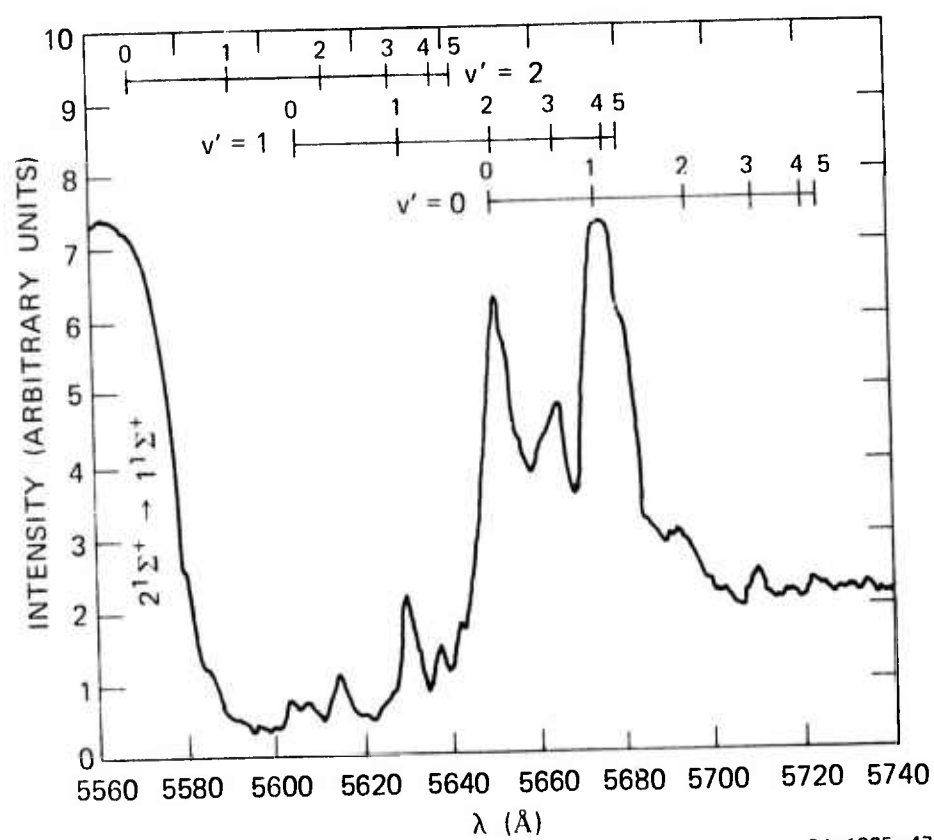
Herman and Herman (HH50) first reported the observation of a continuum emission band centered about 3080 \AA in their xenon-oxygen discharge. They also observed the 2972 \AA atomic transition $O(^1S_0) \rightarrow O(^3P_1)$. Similar observations were made by Cunningham and Clark (CuC74). At our higher xenon pressures we observe only the single asymmetric continuum band (a densitometer trace of which is shown in figure 8). We find that the total emission over the uv band is approximately 1/12 of the total green band emission. Such a continuum is commonly attributed to a transition that terminates on a dissociate lower state. We have interpreted this continuum as the molecular transition in XeO corresponding to the 2972 \AA atomic transition. The transition is red shifted due to the binding of the

1	2	3	4	5	$v' = 2$
				1	
0					
		2	3	4	5
					$v' = 1$
				1	
		2	3	4	
					$v' = 0$



SA-1925-50

FIGURE 6 PHOTOGRAPHIC DISPLAY OF THE MINOR GREEN BAND EMISSIONS OF XeO



SA-1925-47

FIGURE 7 DENSITOMETER TRACE OF THE XeO MINOR GREEN BAND SYSTEM

TABLE I

 $2^1 + \rightarrow 1^1_{\Pi}$ BANDS OF XeO

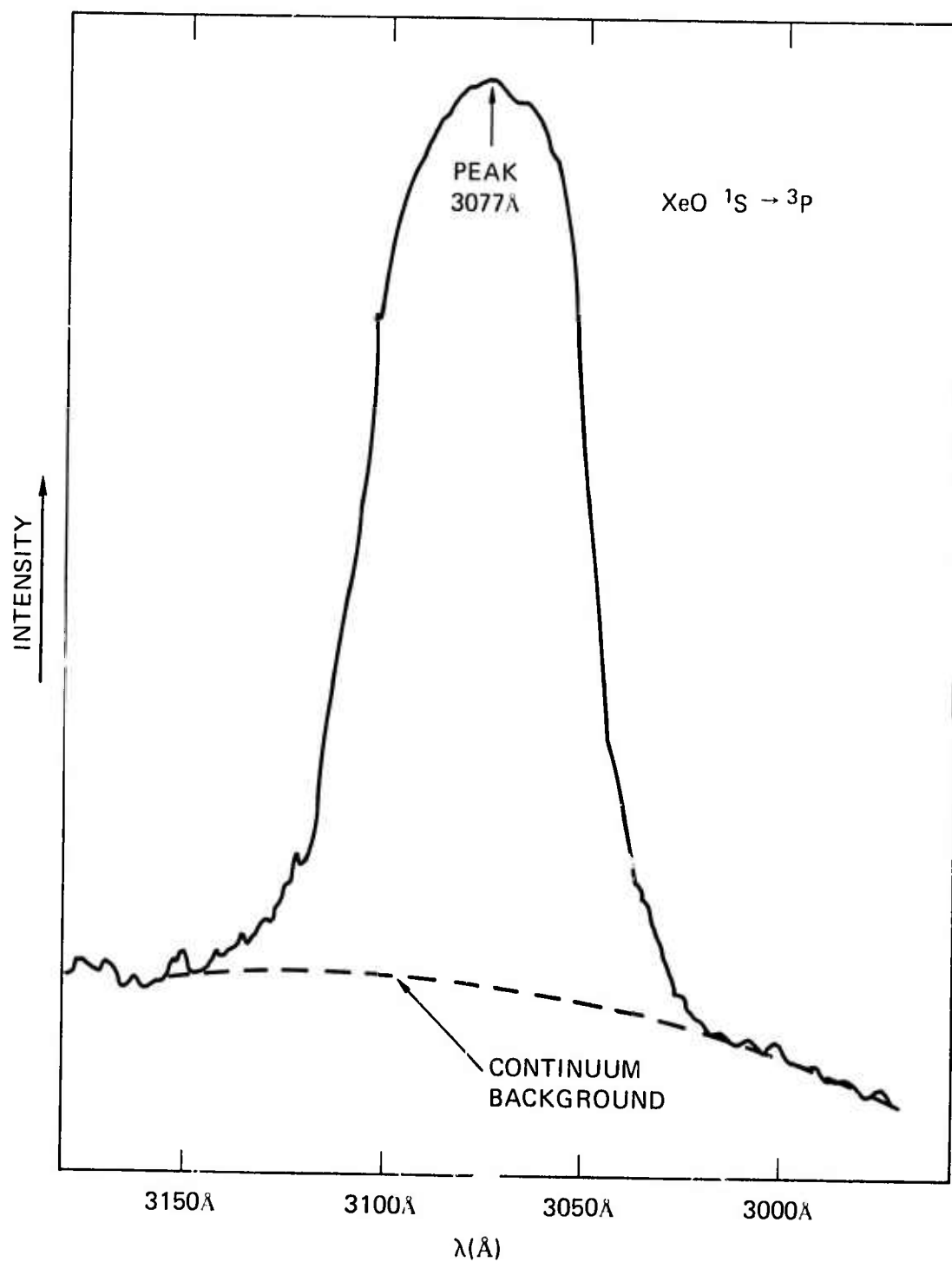
$\lambda(\text{\AA})$	$\nu(\text{cm}^{-1})$	$\nu'\nu''$	I (a)
5719	17486	0,4	ew
5709	17516	0,3	vw
5693	17565	0,2	w
5679	17609	1,5	s
5675	17621	1,4	vs
5673	17627	0,1	vs
5667	17646	1,3	m
5651	17696	1,2	m
5649	17702	0,0	vs
5641	17727	2,5	vw
5637	17740	2,4	w
5631	17759	1,1	m
5629	17765	2,3	m
5614	17812	2,2	w
5606	17836	1,0	vw
5602	17850	3,3	vw
5595	17873	2,1	ew

(a) vs = very strong, s = strong, m = medium, w = weak,
vw = very weak, ew = extremely weak

TABLE II

DESLANDRES TABLE FOR THE $2^1\Sigma \rightarrow 1^1\Pi$ BANDS OF XeO

$v'' \backslash v'$	0	1	2
0	17702 (136) (75)	17838 (79)	
1	17627 (135) (62)	17759 (114) (63)	17823 (61)
2	17565 (131) (49)	17696 (116) (50)	17812 (47)
3	17516 (133) (30)	17646 (119) (25)	17765 (25)
4	17486 (132)	17621 (112) (12)	17740 (13)
5		17609 (115)	17727



SA-1925-112

FIGURE 8 DENSITOMETER TRACE OF XeO UV CONTINUUM

upper state, $2^1\Sigma^+$ ($D_0 = 450 \text{ cm}^{-1}$), and the rise of the repulsive lower state, probably 3Π from $\text{Xe} + \text{O}(^3\text{P})$. From the magnitude of the red shift we can conclude that in the Franck-Condon region the lower state is about 800 cm^{-1} above the $\text{Xe} + \text{O}(^3\text{P}_2)$ separated atom limit.

Potential Curves for XeO

From these spectroscopic data we can now attempt to construct approximate, and at least semiquantitative, potential curves. From the ω_e , $\omega_e x_e$ and D_0 values for each state we can construct Morse potentials. The relative values for R_e for each state can be estimated by eyeball adjustment of the vibrational turning points to get Franck-Condon factors consistent with the observed emission intensities. This procedure may be made somewhat inaccurate by the probable dependence of the electronic transition moment on the internuclear distance. The Morse curves for the bound levels that result are shown in Figure 9.

In the absence of a satisfactory rotational analysis, the absolute internuclear distance scale must be obtained from the repulsive curves. Abrahamson (Ab69) has provided exponential approximations to Thomas-Fermi-Dirac/Born-Mayer repulsive potentials for diatomic molecules. For $\text{Xe} + \text{O}(^3\text{P})$ his tables give $V(R) = 8590e^{-3.65R}$ (V in eV, R in Å). We might use such a potential to describe the lower state of the XeO uv band.

To justify such a procedure we may examine the similar potential for ArO. Recent ab initio calculations of the low lying levels of ArO have been performed by Stevens (St74). His calculations show that the potential curves for the $\text{ArO}(^3\Pi)$ and $\text{ArO}(^3\Sigma^-)$ are both nearly exponential, with the same exponent, and but with the $^3\Sigma^-$ being approximately a factor of 1.7 higher than the $^3\Pi$. Abrahamson's exponential approximation

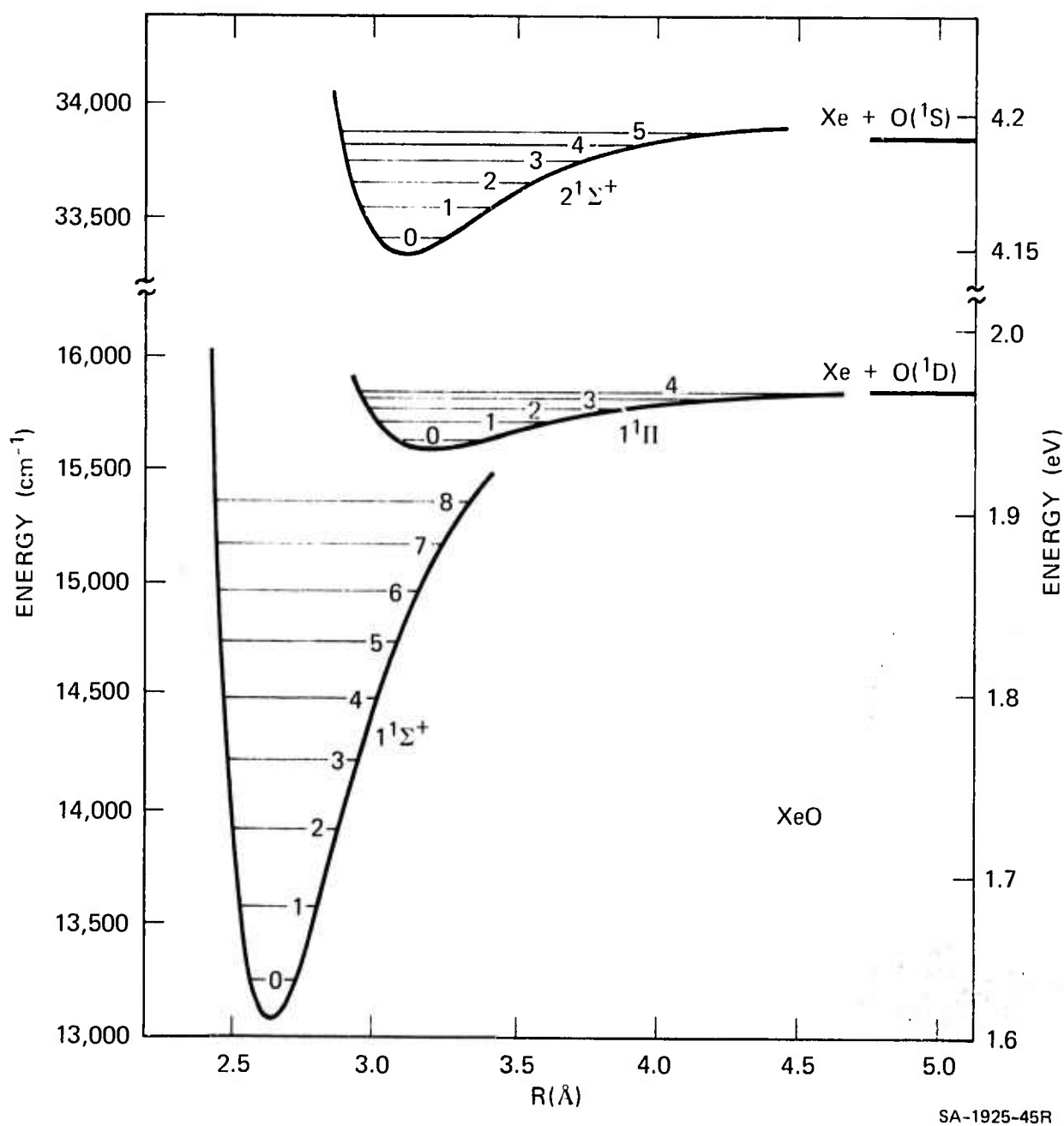
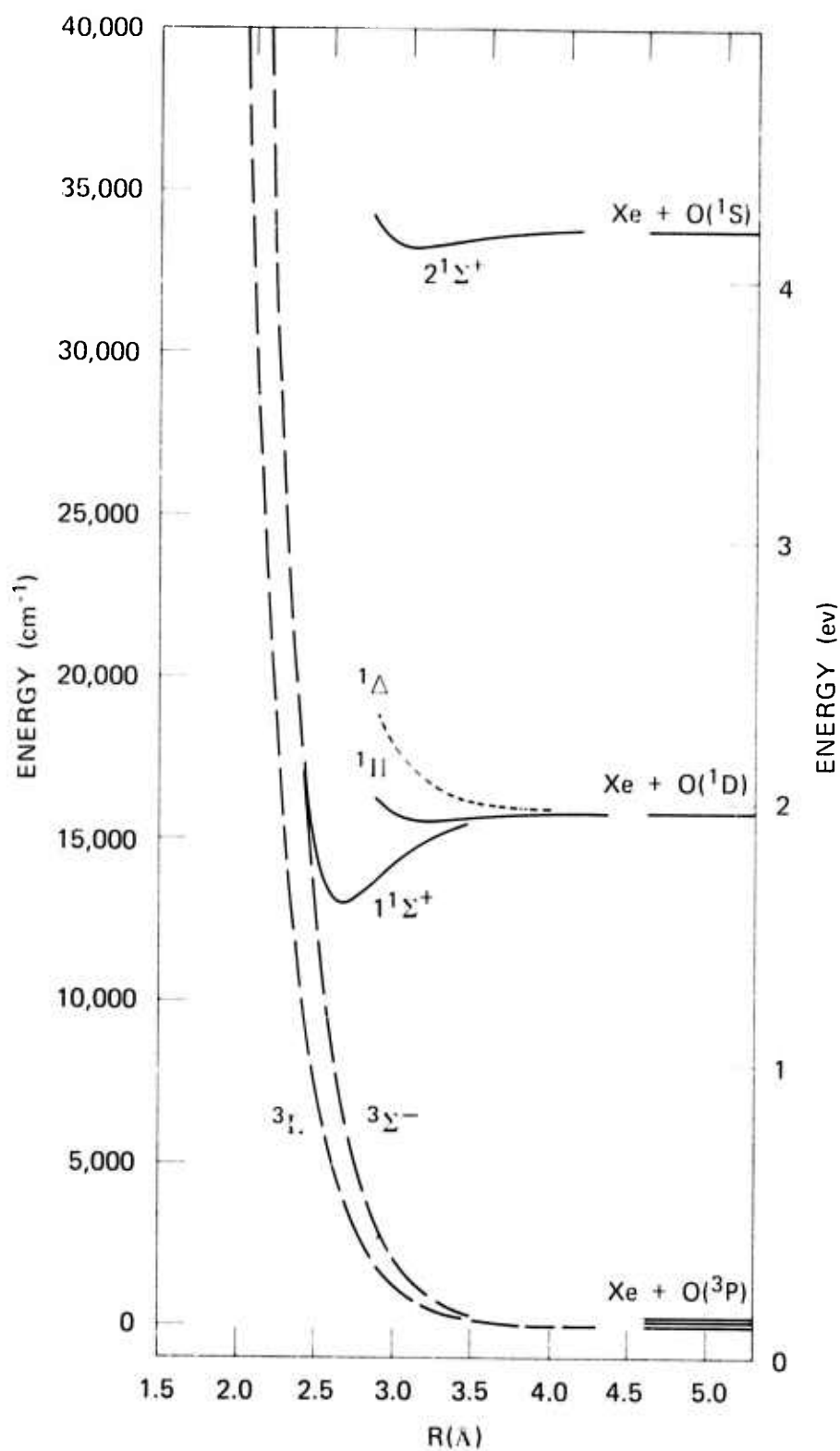


FIGURE 9 MORSE POTENTIALS FOR THE LOW-LYING BOUND SINGLET STATES OF XeO

falls between the two ab initio curves, and on a logarithmic scale is nearly parallel to them.

For XeO we choose the Abrahamson exponential as the potential for the $\text{XeO}(1^3\Pi)$. The $\text{XeO}(1^3\Sigma^-)$ is chosen to be 1.7 times as repulsive in analogy with ArO. To fix the internuclear scale for the bound states we choose the point where the $\text{XeO}(1^3\Pi)$ is 800 cm^{-1} above the $\text{Xe} + \text{O}(^3P_2)$ asymptote and place the equilibrium internuclear separation of the $\text{XeO}(2^1\Sigma^+)$ at that distance. The various potential curves are shown in Figure 10, and the parameters of the bound states are given in Table III. The repulsive $\text{XeO}(1^1\Pi)$ state has been given the same parameters as $1^1\Sigma$ but moved to the $\text{O}(^1D)$ asymptote. Subsequent to the construction of these potential curves, the recent experimental work by Forman et al (FLR74) has suggested that the potential curves of Abrahamson for XeO may need to be shifted inward by approximately 0.2 \AA . According to the prescription used here, the same inward shift would be applied to the bound states as well. Our failure to include the Xe-O Van der Waals interaction and spin-orbit coupling also introduces some inaccuracy to the calibration of the internuclear distance. The need for a rotational analysis is apparent.



SC-1925-55

FIGURE 10 SEMIQUANTITATIVE POTENTIAL CURVES FOR THE LOW-LYING STATES OF XeO

Table III

SPECTROSCOPIC CONSTANTS FOR SINGLET

STATES OF XeO ^a					
State	T_e^b	ω_e	$\omega_e x_e$	R_e^c	D_o
$2^1\Sigma^+$	33268	153	10	3.1	450
$1^1\Pi$	15600	97	8.7	3.2	222
$1^1\Sigma^+$	13068	372	12	2.65	2617

a. energies in cm^{-1} , R_e in \AA

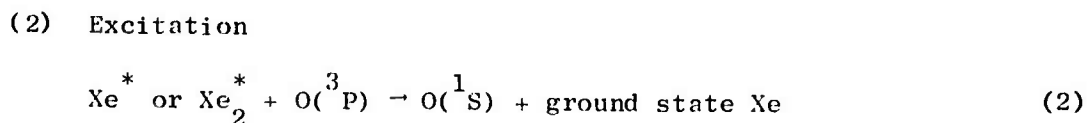
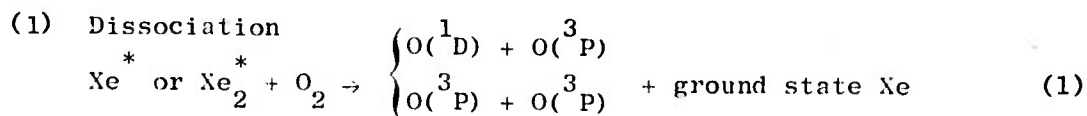
b. above Xe + O(3P_2)

c. based on eyeball relative adjustment of Morse potentials
referenced to Abrahamson repulsive potential (Ab69)

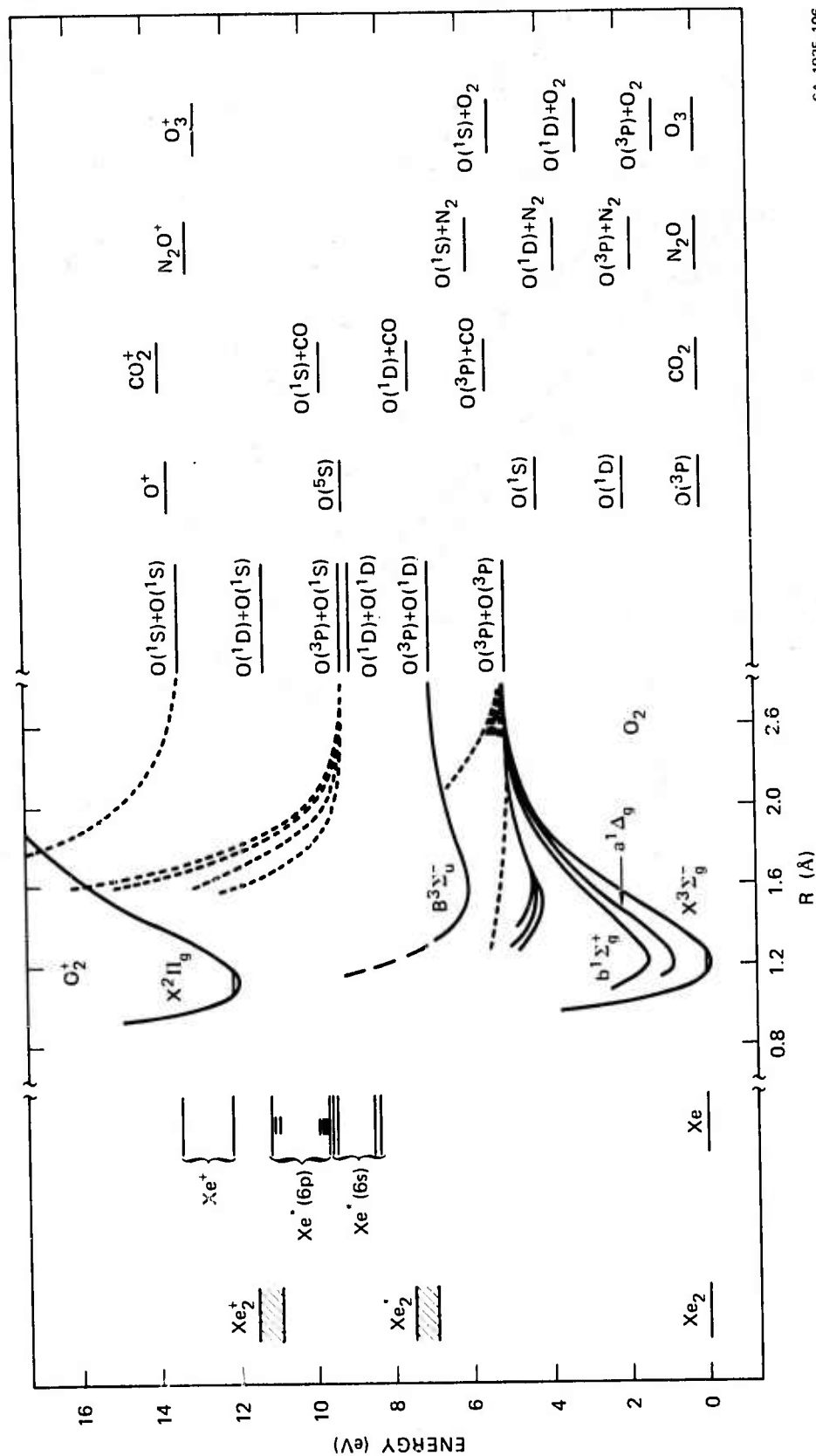
PRODUCTION OF $O(^1S)$ IN XENON/OXYGEN MIXTURES

The bright emissions observed indicate that high densities of $O(^1S)$ are produced. The mechanism of this production is in no way conspicuous. Of particular interest is the observation of similar production efficiencies in Xe/O_2 , Xe/N_2O and Xe/CO_2 , but negligible production in Xe/CO (KANPP46, Ti73, Ti74). Some of the pertinent energy levels are shown in Figure 11. We notice immediately that the energy stored in $Xe^*(^3P_{1,2})$ or Xe_2^* is insufficient to produce $O(^1S)$ by direct dissociative excitation of O_2 and CO_2 . Tisone (Ti73) suggested that transfer from the more energetic $Xe^*(^3P_0)$ might produce $O(^1S)$ in a single step. Inspection of Figure 11 suggests that even the higher levels of Xe^* would have difficulty reaching the curves that dissociate to $O(^1S)$. Further, $Xe^*(^3P_0)$ is not sufficiently energetic to give $O(^1S)$ from CO_2 .

On the basis of our kinetic studies we believe that the most plausible excitation scheme involves two energy transfer reactions:

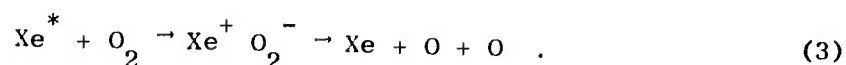


Recent work by Velazco and Setser (VS74) indicates that energy transfer from Xe^* to O_2 occurs readily ($k = 2.2 \times 10^{-10} \text{ cm}^3/\text{sec}$). One would expect this reaction to be mediated by the charge transfer channel



SA-1925-106

FIGURE 11 SELECTED ENERGY LEVELS FOR Xe, O₂, O, CO₂, N₂O, O₃

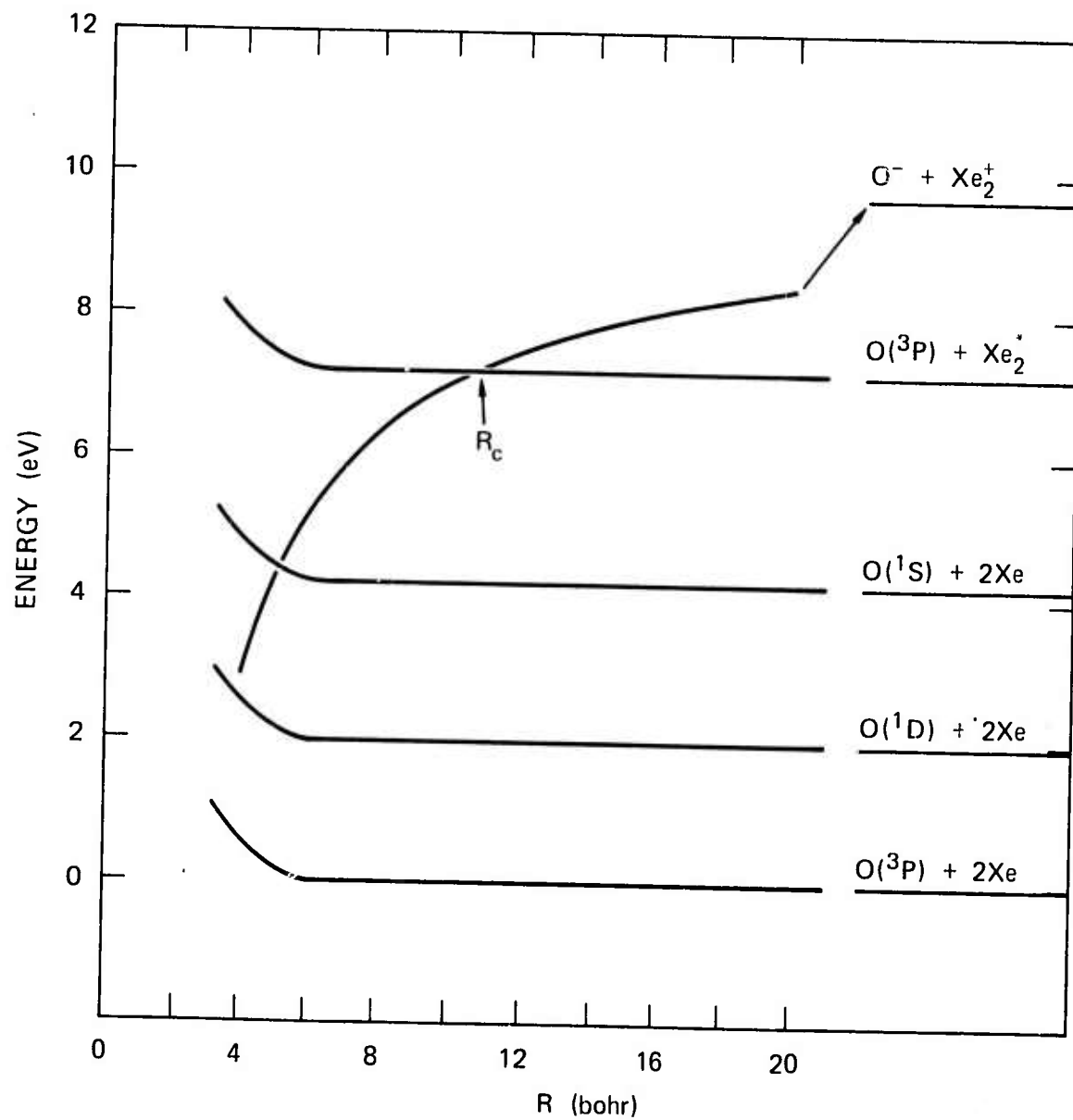


The crossing of the neutral and ionic surfaces at $R_c = 7.8 a_0$ would suggest a quenching rate coefficient ($k \approx \bar{v} \pi R_c^2$) of $3 \times 10^{-10} \text{ cm}^3/\text{sec}$. Energy transfer from Xe_2^* should also proceed through an ionic intermediate, with a similar rate coefficient.

Energy transfer to $\text{O}(^3\text{P})$ might seem less likely due to the lack of suitably resonant energy levels. Once again we would expect an ionic intermediate to be important. The potential curves are sketched in Figure 12, for the case of $\text{Xe}_2^* + \text{O}(^3\text{P})$. Production of $\text{O}(^1\text{S})$ is the nearest exothermic channel for energy transfer. The reactants approach until the ionic potential surface is reached. Electron transfer puts the reaction onto the ionic surface. The electron is returned when the final product surface is reached. The initial crossing at $R_c = 10.8 a_0$ leads irreversibly to energy transfer with a rate coefficient of 5.7×10^{-10} . Energy transfer from Xe^* , which has nearly the same ionization potential as Xe_2^* , should proceed nearly as rapidly.

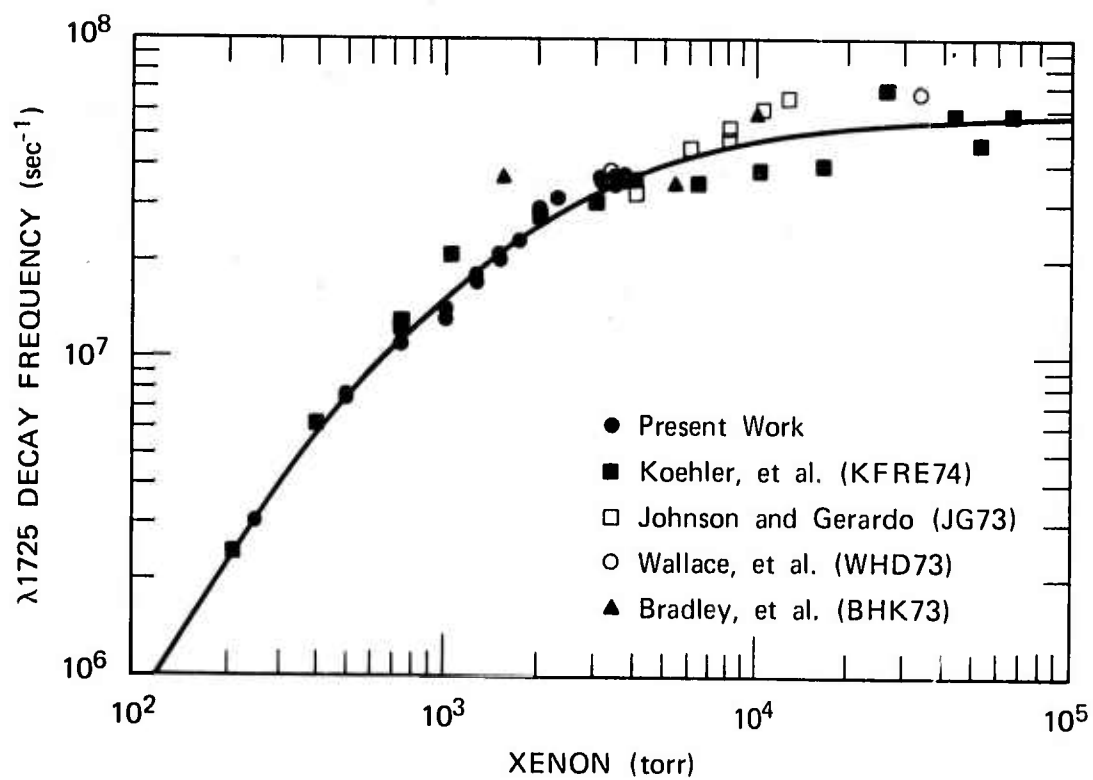
Quenching of Xe_2^*

To investigate the energy pathways in some greater detail we measured the quenching by O_2 of the Xe_2^* fluorescence in the region of 1720-5 Å. An adequate reference point was obtained by first studying the pressure dependence of this fluorescence in pure xenon. In a previous report (LEH73) we discussed the pressure dependence of the apparent radiative lifetime of Xe_2^* . To provide more accurate values in the pressure region of current interest, we have observed the Xe_2^* decay frequency for xenon pressures from 250 to 3900 torr. Figure 13 shows the full range of values now available at high excitation



SA-1925-109R

FIGURE 12 SCHEMATIC POTENTIAL CURVES FOR ENERGY TRANSFER
FROM Xe_2^+ TO $O(^3P)$



SA-1925-95

FIGURE 13 PRESSURE DEPENDENCE OF XENON EXCIMER RADIATIVE DECAY FREQUENCY ($10^2 - 10^5$ torr)

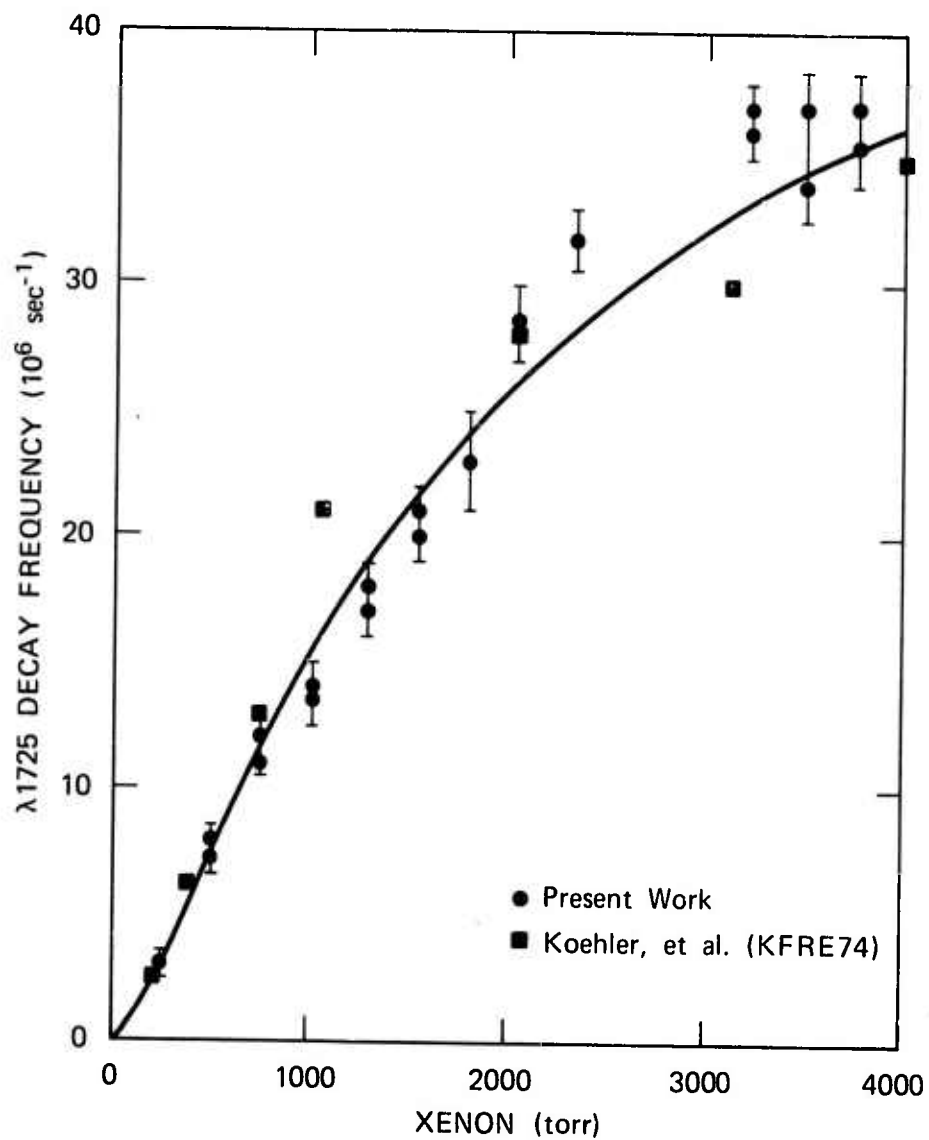
densities. Figure 14 shows the decay frequency for the 0 to 4000 torr pressure range.

The operation of the proposed two-step scheme for producing $O(^1S)$ will depend strongly on the number of excimers or metastables available for energy transfer. Furthermore, determination of the efficiency will require a knowledge of the energy deposition. Simple arguments suggest that the energy deposited should increase approximately linearly with the rare gas density, and slightly faster than linearly with the atomic number. By performing an absolute calibration of the photon flux and integrating the photon flux over the duration of the excimer formation and decay we may determine (in the absence of serious quenching) the total density of excimers produced in a given excitation pulse. Figure 15 shows the result of this procedure. At best, a factor-of-three accuracy can be attributed to the absolute calibration. The linear deposition is well demonstrated, at least over this pressure range. The absolute deposition of 4.8×10^{15} excimers/cm³ per atmosphere in xenon compares well with the value of 1.1×10^{15} used previously (HGHML74) for deposition in argon.

Figure 16 shows the additional quenching of the Xe_2^* excimer fluorescence by added molecular oxygen. The breaks in the decay plots suggest that more than one quenching mechanism is operating. Based on the proposed two-step mechanism one would expect the quenching reaction

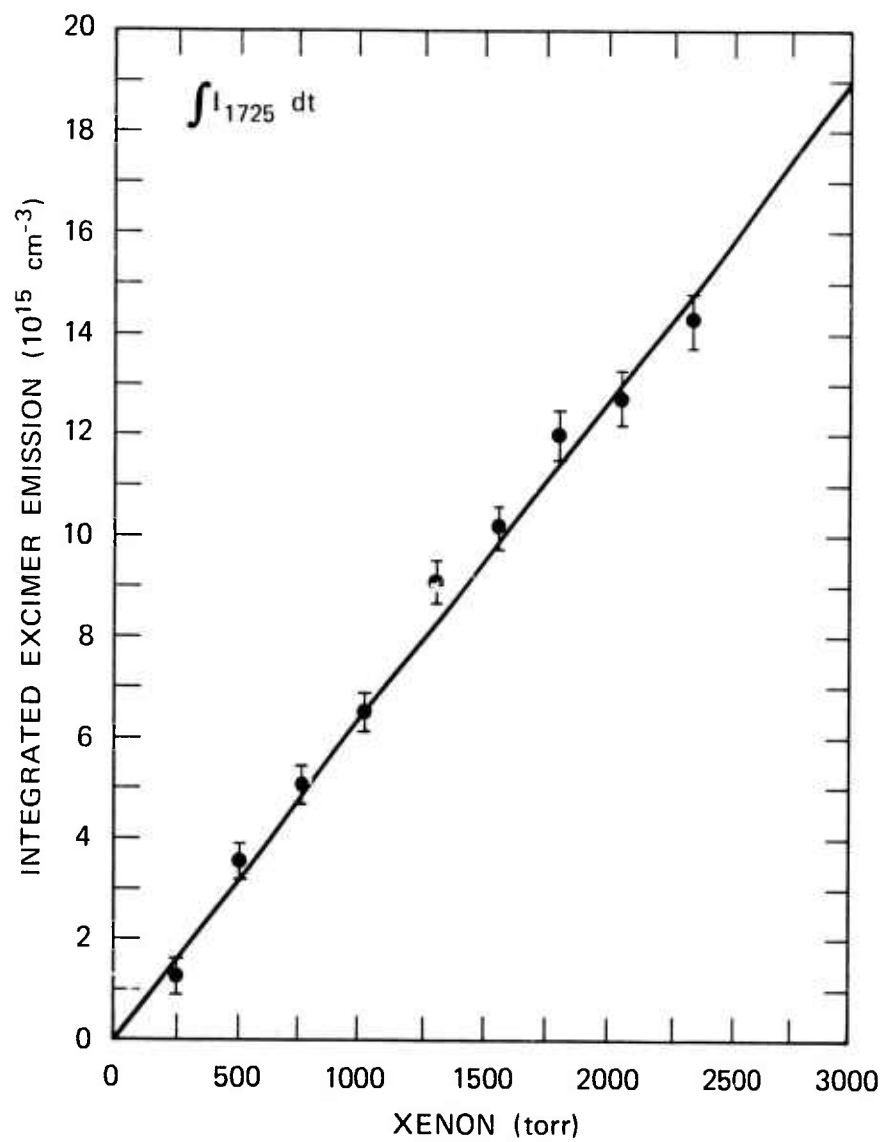


to be dominant at the highest oxygen pressures. One obtains a quenching rate coefficient of $1.5 \pm 0.2 \times 10^{-10}$ cm³/sec by O_2 . If a significant fraction of the O_2 is dissociated through reaction 4, the $O(^3P)$ with



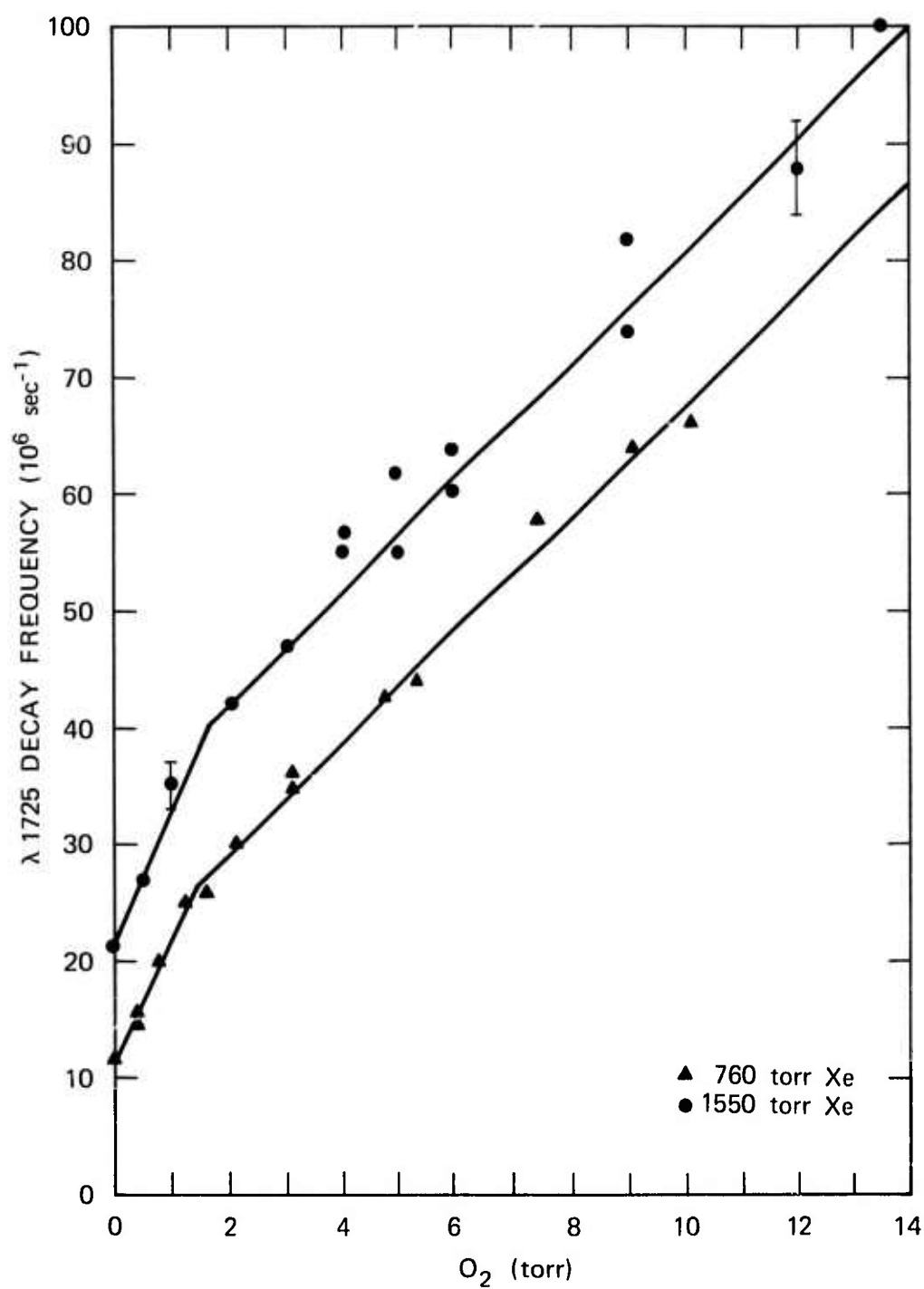
SA-1925-96

FIGURE 14 PRESSURE DEPENDENCE OF XENON EXCIMER RADIATIVE DECAY FREQUENCY (0 - 4000 torr)



SA-1925-97

FIGURE 15 XENON PRESSURE DEPENDENCE OF TIME-INTEGRATED EXCIMER EMISSION



SA-1925-98

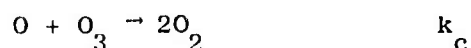
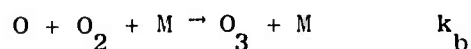
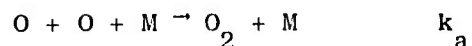
FIGURE 16 OXYGEN QUENCHING OF XENON EXCIMER FLUORESCENCE

its larger expected quenching cross section, can cause a significant loss of Xe_2^* . Indeed, this is necessary if one expects to produce $\text{O}(^1\text{S})$ efficiently. We interpret the low O_2 quenching of Xe_2^* shown in Figure 16 as arising dominantly from quenching by $\text{O}(^3\text{P})$. After we have obtained a measure of the $\text{O}(^3\text{P})$ density (below), a rate coefficient can be determined.

Ozone Formation

Having identified the important role played by ground state oxygen atoms, we sought a more direct means of determining their concentration. As described above, our preliminary kinetic measurements were obscured by the copious production of ozone in xenon/oxygen mixtures repeatedly excited by the Febetron. This should have been obvious since discharged rare gas/oxygen mixtures are often used to produce ozone in macroscopic quantities. Since we used this ozone production as a diagnostic aid, we should examine the kinetics of its formation.

The competing processes are



Johnson (Jo68) gives recommended rate coefficients for these reactions with O_2 as the third body:

$$k_a(\text{O}_2) = 3.80 \times 10^{-30} T^{-1} \exp(-170/T) \text{ cm}^6/\text{sec}$$

$$k_b(\text{O}_2) = 4.63 \times 10^{-35} \exp(1050/T) \text{ cm}^6/\text{sec}$$

$$k_c = 2.00 \times 10^{-11} \exp(-2395/T) \text{ cm}^3/\text{sec}$$

Setting $T = 300^{\circ}\text{K}$, and assuming that xenon is approximately 1/3 as effective a collision partner as O_2 , we obtain

$$k_a(\text{Xe}) \approx 2.4 \times 10^{-33} \text{ cm}^6/\text{sec}$$

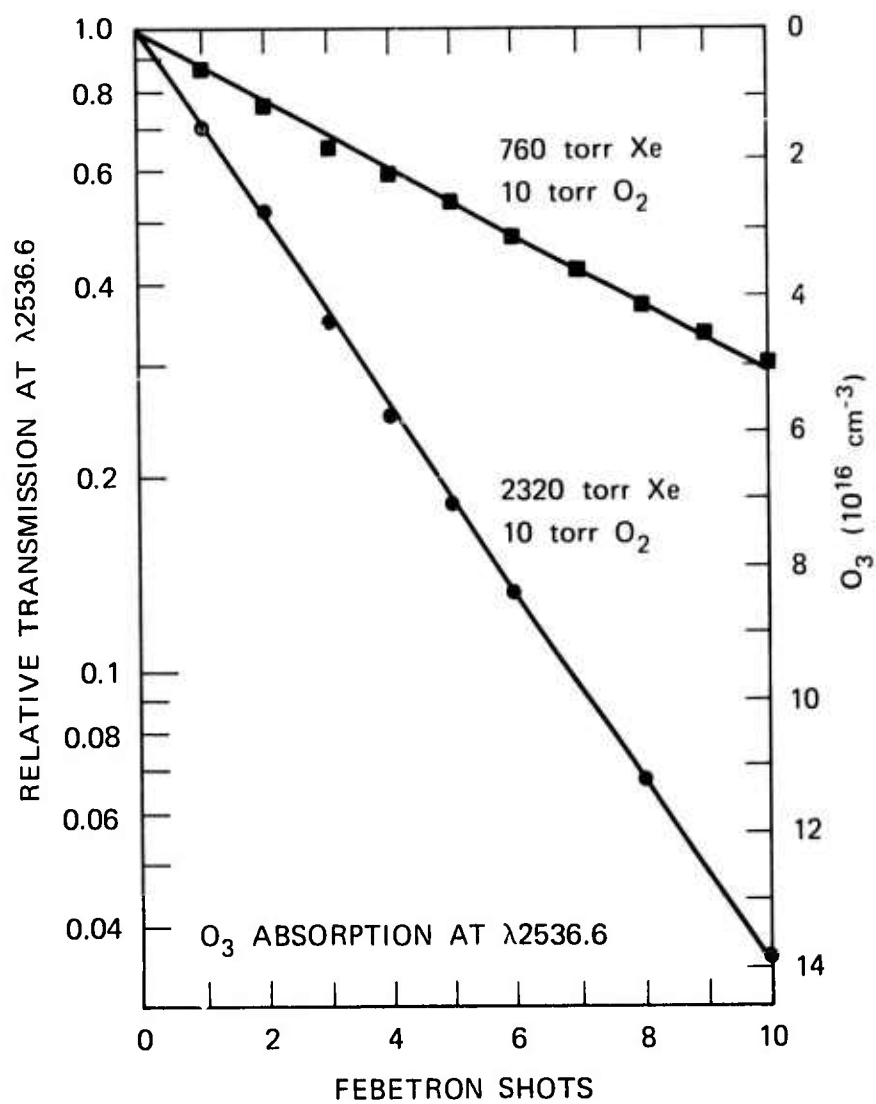
$$k_b(\text{Xe}) \approx 5.1 \times 10^{-34} \text{ cm}^6/\text{sec}$$

$$k_c = 6.8 \times 10^{-15}$$

Detailed solution of the kinetic equations will not be necessary at this time. For comparison with experimental data to be presented below, we consider the case of 10 torr O_2 in 1 atm Xe with 1% initial dissociation of the O_2 into $\text{O}(^3\text{P})$. The dominant reaction should be $\text{O} + \text{O}_2 + \text{Xe}$, which would consume the free oxygen atoms in about 300 μsec , with about 95% conversion into O_3 . Under these conditions we would expect the final ozone concentration to be nearly the same as the initial concentration of $\text{O}(^3\text{P})$. At higher initial dissociation fractions or high initial concentrations of O_3 the conversion of $\text{O}(^3\text{P})$ to O_3 becomes more complicated and less efficient.

To determine the amount of ozone actually produced in Febetron excited oxygen mixtures, the transmission of the 2537 \AA Hg line through the gas cell was measured after each shot. The data are shown in Figure 17. From a knowledge of the O_3 absorption cross section at 2537 \AA ($\sigma = 1.2 \times 10^{-17} \text{ cm}^2$ from WZI53) and assuming an absorption length of 2 cm, the concentration of O_3 can be determined.

We find that at a xenon pressure of 1 atmosphere, each Febetron shot results in the production of $5.2 \times 10^{15} \text{ O}_3/\text{cm}^3$. At three atmospheres we obtain $1.4 \times 10^{16} \text{ O}_3/\text{cm}^3$ per shot. Comparison with Figure 15 indicates that one would have expected 9.6×10^{15} and 2.9×10^{16} , respectively, to be the ozone densities if each Xe_2^* dissociated one O_2 . Based



SA-1925-94

FIGURE 17 OZONE PRODUCTION IN FEBETRON EXCITED XENON/OXYGEN MIXTURES

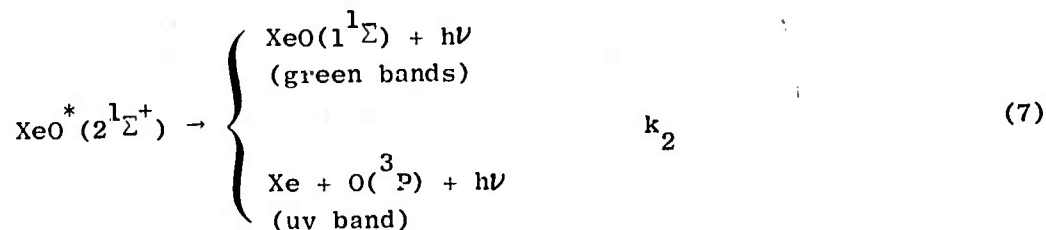
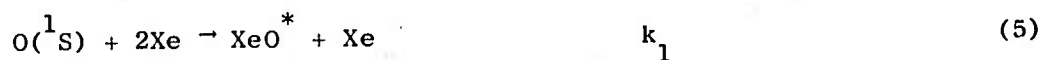
on our interpretation of the quenching of Xe_2^* by O_2 (see Figure 16) and quantified by the kinetic model described below, some of the Xe_2^* excimers are lost by radiation and some by energy transfer to $\text{O}({}^3\text{P})$. This yields reduced estimates of $7.8 \times 10^{+15}$ and $1.8 \times 10^{16} \text{ O}_3/\text{cm}^3$ at one and three atmospheres, respectively. Remembering the difficulties in making absolute calibrations (especially estimating the active volume), we will be satisfied with this level of agreement.

THE DECAY OF XeO

The tendency of $O(^1S)$ to form the weakly bound XeO excimer greatly complicates the analysis of the decay kinetics. From the magnitude of the binding energy (450 cm^{-1}) one may estimate the relative number that are bound at thermal equilibrium. Our calculations, as well as those of Atkinson and Welge (AW74), indicate that even at a xenon pressure of one atmosphere only about 1.4% of the $O(^1S)$ atoms are bound as XeO excimers. Some care will be necessary to separate the effects of quenching XeO from those of quenching $O(^1S)$.

Several previous studies (CuC74, AW74, FSW70, HO70, Ti73, Ti74) have followed the fluorescence and decay of $O(^1S)$ in low pressure xenon. The recent work by Cunningham and Clark (CuC74) and Atkinson and Welge (AW74) have shown that most, if not all, of the apparent collisional deactivation of $O(^1S)$ by xenon proceeds through the formation of XeO, which subsequently radiates very rapidly.

In general the equations describing the decay of $O(^1S)$ in Febetron excited xenon/oxygen mixtures may be written as follows





As noted above the spectroscopic data on $\text{XeO}(2^1\Sigma^+)$ may be used to calculate the association-dissociation equilibrium constant $K = k_1/k_{-1} = 5.5 \times 10^{-22} \text{ cm}^3$.

At xenon pressures less than 10 atm, the XeO concentration is much less than the concentration of free $\text{O}(^1\text{S})$ atoms. Therefore, one cannot follow the radiative decay of XeO directly. Rather, one observes that the emission appears to be "collisionally induced." This may be described by the reaction $\text{Xe} + \text{O}(^1\text{S}) \rightarrow \text{Xe} + \text{O}(^1\text{D}) + h\nu$, with an effective two-body rate coefficient k_R . The range of values for this rate coefficient which have been obtained in various laboratories are shown in Table IV. The difficulties involved in temperature control in discharges (CuC74) and very high intensity e-beam excited gases (PMR74b) may explain the low values obtained under these conditions. Atkinson and Welge (AW74) found that at 201°K the rate coefficient had increased to $6.8 \pm 0.8 \times 10^{-15} \text{ cm}^3/\text{sec}$, consistent with the temperature change in the equilibrium constant $\sim \exp\{+450 \text{ cm}^{-1}/kT\}$. At 400°K one would expect the equilibrium constant to drop to about $\frac{1}{2}$ of its room temperature value. If we accept a value of $4.0 \pm 0.5 \times 10^{-15} \text{ cm}^3/\text{sec}$ at room temperature, then the radiative lifetime of $\text{XeO}(2^1\Sigma^+)$ would be

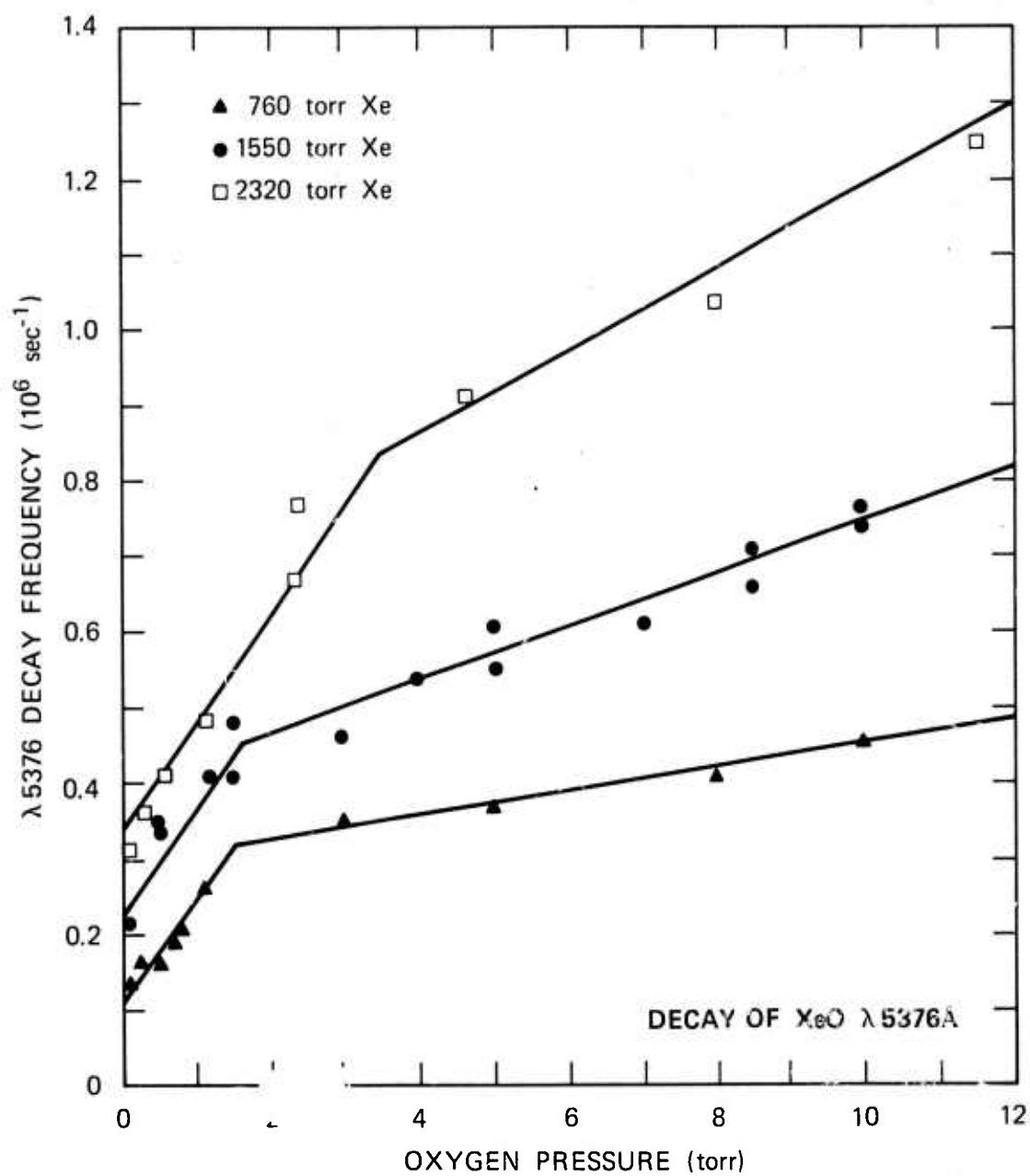
$$\tau = K/k_R = 5.5 \times 10^{-22} / 4 \times 10^{-15} = 140 \pm 20 \text{ nsec.} \quad (12)$$

Figures 18 and 19 show the decay frequency at 5376 \AA of various Febetron-excited xenon/oxygen mixtures as observed in our laboratory.

Table IV

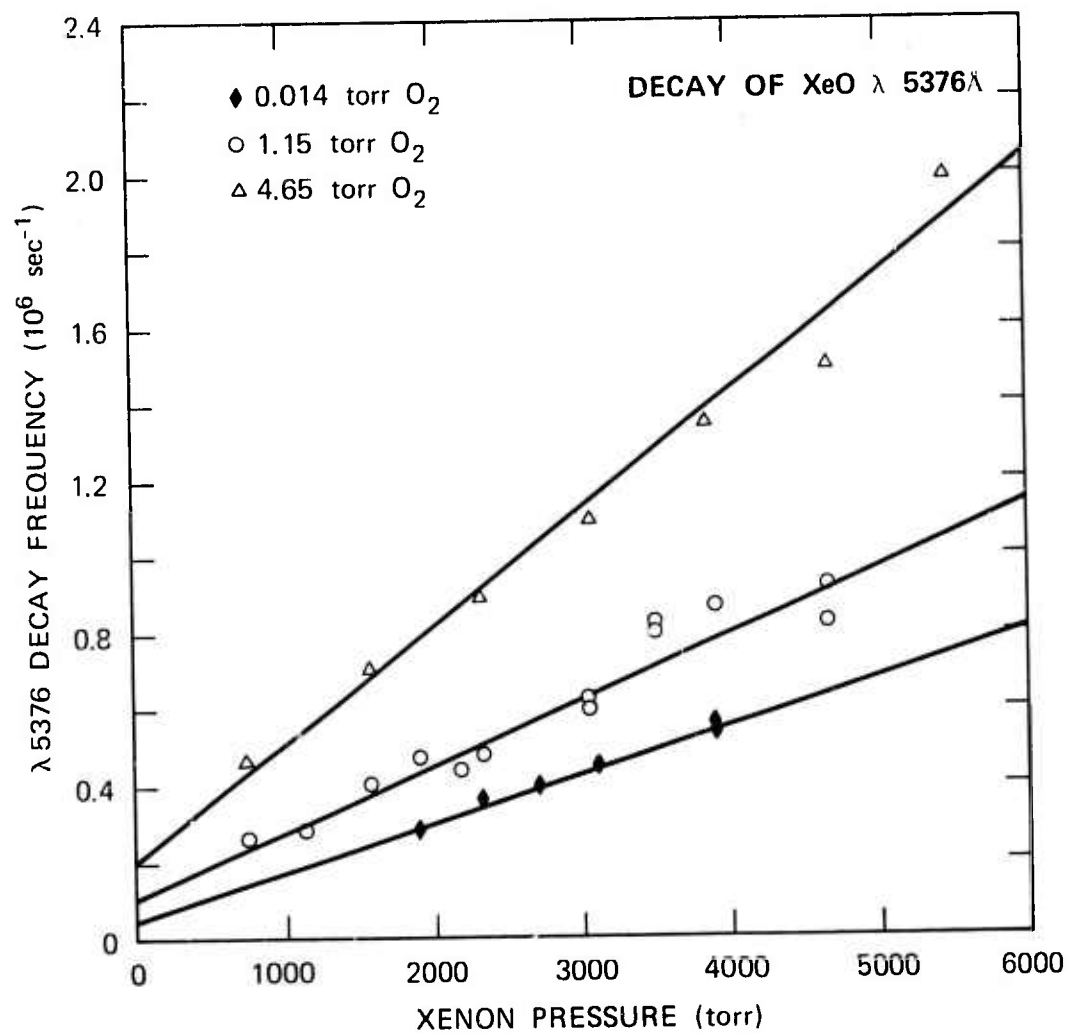
Rate Coefficients for
Collision-Induced Emission of $O(^1S)$ by Xe

<u>k_R (cm³/sec)</u>	<u>Observed</u>	<u>Reference</u>
6.7×10^{-15}	decay	FSW70
1.7×10^{-15}	intensity	CuC74
3.7×10^{-15}	intensity	AW74
3.6×10^{-15}	decay	AW74
2.0×10^{-15}	decay	PMR74b
4.0×10^{-15}	decay	present work



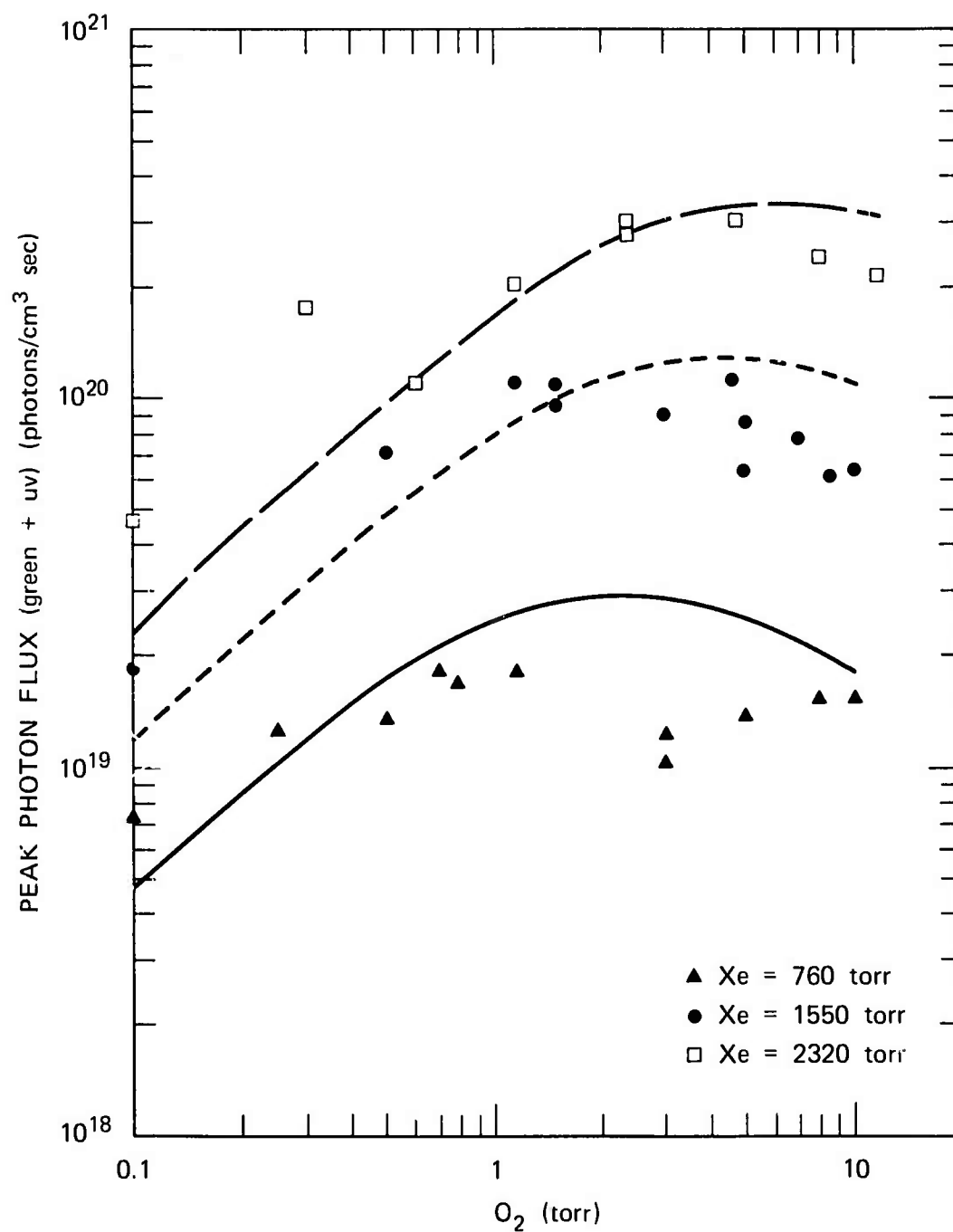
SA-1925-99

FIGURE 18 OXYGEN PRESSURE DEPENDENCE OF XeO DECAY



SA-1925-100

FIGURE 19 XENON PRESSURE DEPENDENCE OF XeO DECAY



SA-1925-111

FIGURE 20 OXYGEN PRESSURE DEPENDENCE OF XeO FLUORESCENCE INTENSITY COMPARED WITH PRELIMINARY KINETIC MODEL

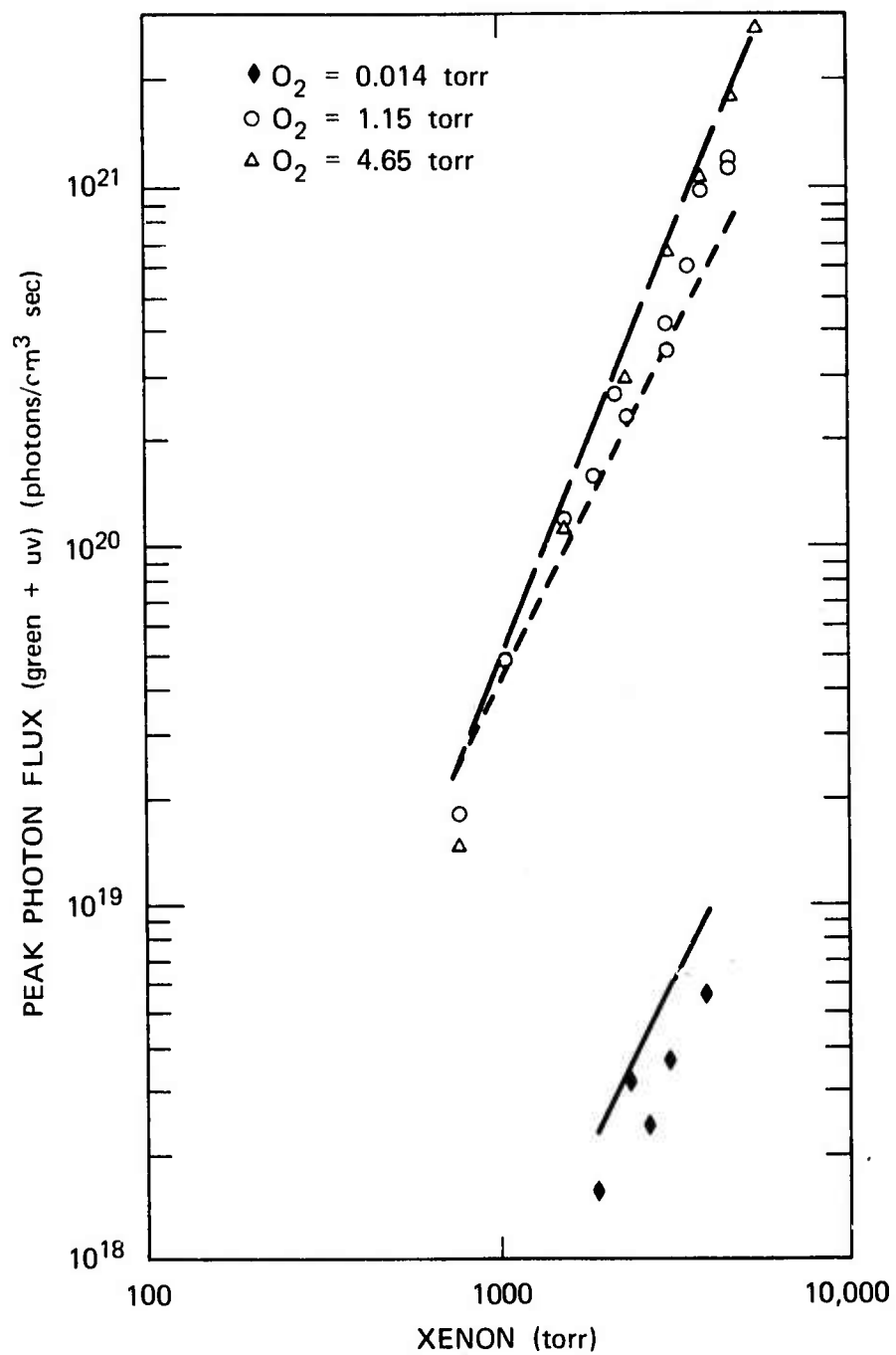


FIGURE 21 XENON PRESSURE DEPENDENCE OF XeO FLUORESCENCE INTENSITY COMPARED WITH PRELIMINARY KINETIC MODEL

The lines drawn through the data are not yet representative of any kinetic fit, rather they merely indicate the trends that must be explained by the kinetic model.

Figures 20 and 21 show plots of the observed peak XeO fluorescence intensities. We can see that at low O_2 densities the intensity increases as the first power of O_2 and between the second and third power in Xe. At higher O_2 pressures the intensity begins to decrease. In view of the proposed scheme for production and decay of $O(^1S)$ these intensity data may be explained as follows:

- (1) At low O_2 pressure most of the Xe_2^* is lost by radiation. The amount of energy transfer is proportional to the O_2 pressure.
- (2) At intermediate O_2 pressure some fraction of the Xe_2^* results in excitation of $O(^3P)$ to $O(^1S)$.
- (3) At high O_2 pressure most of the Xe_2^* is lost through dissociation of O_2 .
- (4) The XeO intensity is proportional to the xenon pressure through the $XeO \rightleftharpoons Xe + O(^1S)$ equilibrium.
- (5) The amount of $O(^3P)$ produced is proportional to the energy deposition [i.e., xenon pressure].
- (6) The fraction of the $O(^3P)$ that is converted to $O(^1S)$ is also proportional to the energy deposition.

Hence, as further amplified below, in the discussion of the kinetic model, we expect the XeO intensity to vary as

$$I_{XeO} \sim [Xe]^3 [O_2] \cdot \left(\frac{1}{k_7 + k_5 [O_2]} \right)^2, \quad (13)$$

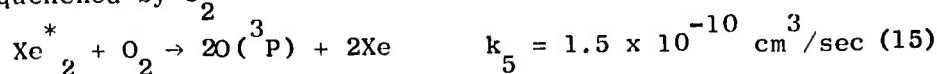
where k_5 is the rate coefficient for quenching of Xe_2^* by O_2 , and k_7 is the pressure dependent radiative lifetime of Xe_2^* (see Figures 13-14). The theoretical intensity curves drawn with the experimental data points in Figures 20 and 21 are results from our preliminary model calculations. Essentially, we have just used equation 13 with the measured kinetic rate coefficients.

THE KINETIC MODEL

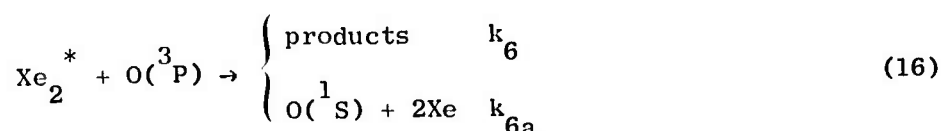
We present below a kinetic model for the formation and decay of $O(^1S)$ and XeO in Febetron excited xenon/oxygen mixtures. Certain simplifications have been made that allow a closed form solution. The intent has been to identify the physically important reaction as a starting point for more exacting experimental verification and more refined model calculations. Initially we assume an instantaneous source of Xe_2^*

$$[Xe_2^*]_{t=0} = 4.8 \times 10^{15} \text{ cm}^{-3} \text{ per atmosphere} \quad (14)$$

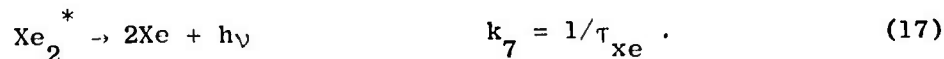
which may be quenched by O_2



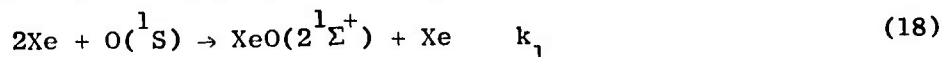
or by $O(^3P)$



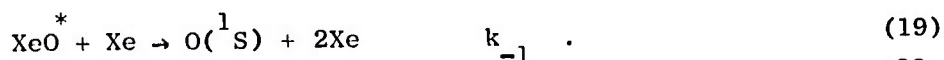
Finally if the Xe_2^* fails to find a collision partner, it may radiate



As described above, the $O(^1S)$ produced may form the XeO excimer

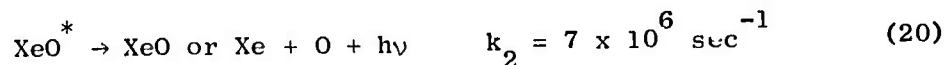


which can then be dissociated again

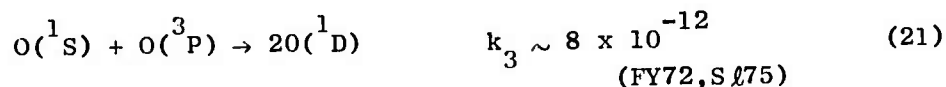


At room temperature the equilibrium constant is $K = k_1/k_{-1} = 5.5 \times 10^{-22}$

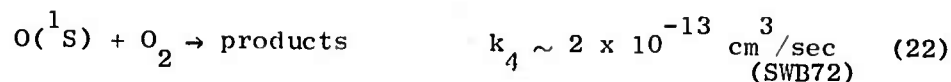
If left to their own devices, the XeO molecules may radiate



More likely is the quenching of the dominant excited oxygen species by $O(^3P)$



Except at low excitation densities, quenching by O_2



is much less important. Because of its much lower density direct quenching of XeO by O_2 or $\text{O}(^3\text{P})$ is also likely to be unimportant. This kinetic scheme is illustrated in the energy flow chart, Figure 22.

We begin with the degradation of the energy stored in Xe_2^* .

Defining the shorthand notation

$$X \equiv [\text{Xe}_2^*], \quad O \equiv [\text{O}(^3\text{P})], \quad S \equiv [\text{O}(^1\text{S})] \quad (23)$$

the energy flow equations may be written

$$\frac{dX}{dt} = -k_7 X - k_6 OX - k_5 O_2 X \quad (24)$$

$$\frac{dO}{dt} = +2k_5 O_2 X - k_{6a} OX \quad (25)$$

$$\frac{dS}{dt} = +k_{6a} OX \quad (26)$$

Each of these equations is nonlinear in the time-dependent concentrations, so that the system does not have an exponential solution. However, a change of variables can linearize the equations. Specifically we define a new time variable y such that

$$\frac{d}{dt} = X \frac{d}{dy} \rightarrow y = \int_0^t X(t') dt' \quad (27)$$

Then we find that

$$\frac{dX}{dy} = -k_7 - k_6 O - k_5 O_2 \quad (28)$$

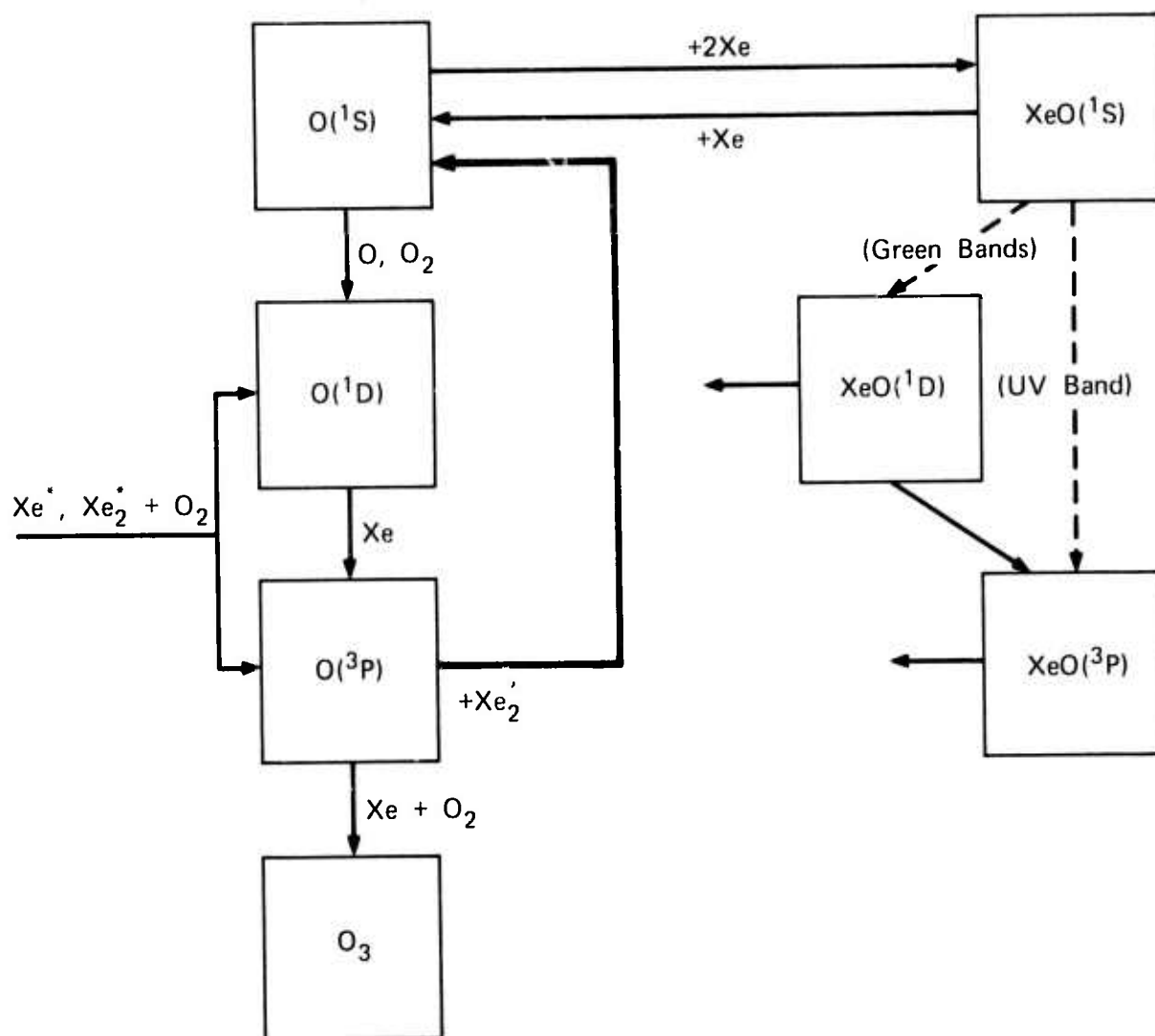
$$\frac{dO}{dy} = +2k_5 O_2 - k_{6a} O \quad (29)$$

$$\frac{dS}{dy} = k_{6a} O \quad (30)$$

Further we note that the number of oxygen atoms must be conserved, this yields

$$2O_2 + O + S = \text{const} = 2O_2^0 \quad (31)$$

Substitution of this relation yields



SA-1925-101R

FIGURE 22 ENERGY FLOW IN XENON/OXYGEN MIXTURES

$$\frac{dX}{dy} = -k_7 - k_6 O - k_5 [O_2^O - \frac{1}{2}O - \frac{1}{2}S] \quad (32)$$

$$= -k_7 - k_5 O_2^O - (k_6 - \frac{1}{2}k_5)O + \frac{1}{2}k_5 S \quad (33)$$

$$\frac{dO}{dy} = 2k_5 [O_2^O - \frac{1}{2}O - \frac{1}{2}S] - k_{6a} O \quad (34)$$

$$= 2k_5 O_2^O - (k_{6a} + k_5)O - k_5 S \quad (35)$$

$$\frac{dS}{dy} = k_{6a} O . \quad (36)$$

We now proceed to solve these linear, coupled equations.

First, we define the new concentration variables

$$Q = O + S \quad (37)$$

$$R = X + \frac{k_6}{k_{6a}} S . \quad (38)$$

Then the kinetic equations simplify to

$$\frac{dR}{dy} = -k_7 - k_5 O_2^O + \frac{1}{2}k_5 Q \quad (39)$$

$$\frac{dQ}{dy} = 2k_5 O_2^O - k_5 Q \quad (40)$$

For these equations we may immediately write down the solutions

$$Q - Q_0 = 2O_2^O [1 - \exp(-k_5 y)] \quad (41)$$

$$R - R_0 = -k_7 y - O_2^O [1 - \exp(-k_5 y)] . \quad (42)$$

To establish the initial and final conditions we must refer to the change of time-variable from t to y . Specifically

$$\text{at } t = 0.0 \quad y = 0.0, X = X_0, O = 0.0, S = 0.0 \quad (43)$$

$$\text{at } t \rightarrow \infty: y \rightarrow \int_0^\infty X(t)dt = y_f, X \rightarrow 0.0, O \rightarrow O_f, S \rightarrow S_f . \quad (44)$$

Unfolding the relation between Q, W, and S gives

$$O_f = \frac{2k_5^O O_2^O}{k_{6a} - k_5} [\exp(-k_5 y_f) - \exp(-k_{6a} y_f)] , \quad (45)$$

where the subscript f refers to the final density; and

$$S_f = \frac{2O_2^O}{k_{6a} - k_5} \left\{ k_{6a} [1 - \exp(-k_5 y_f)] - k_5 [1 - \exp(-k_{6a} y_f)] \right\} . \quad (46)$$

Finally, the equation for R yields

$$\frac{k_6}{k_{6a}} S_f - X_o = -k_7 y_f - O_2^O [1 - \exp(-k_5 y_f)] \quad (47)$$

We now have solved for the final concentrations of $O(^3P) = O_f$ and $O(^1S) = S_f$ in terms of the rather inconvenient parameter y_f . We would much prefer to have expressions for O_f and S_f in terms of the oxygen and xenon pressures directly. The parameter y_f can, of course, be found implicitly from the expressions for S_f and X_o . Under our actual experimental conditions we find that

$$\frac{k_6}{k_{6a}} S_f \ll X_o, \quad k_5 y \ll 1, \quad \text{and} \quad k_{6a} y \ll 1 \quad (48)$$

which allow the simplifications

$$-X_o \approx -k_7 y_f - O_2^O (k_5 y_f) \quad (49)$$

$$\begin{aligned} O_f &\approx \frac{2k_5^O O_2^O}{k_{6a} - k_5} [(1 - k_5 y_f) - (1 - k_{6a} y_f)] \\ &= 2O_2^O (k_5 y_f) \end{aligned} \quad (50)$$

$$\begin{aligned}
S_f &\approx \frac{2O_2^0}{k_{6a} - k_5} \left\{ k_{6a} \left[1 - (k_5 y_f) + \frac{(k_5 y_f)^2}{2} \right] \right. \\
&\quad \left. - k_5 \left[1 - (k_{6a} y_f) + \frac{(k_{6a} y_f)^2}{2} \right] \right\} \\
&= O_2^0 k_{6a} k_5 y_f^2 .
\end{aligned} \tag{51}$$

From these we may simplify even further, to give

$$y_f \approx \frac{X_o}{k_7 + k_5 O_2} . \tag{52}$$

If we define the effective excitation transfer parameter

$$Z = k_5 y = \frac{k_5 X_o}{k_7 + k_5 O_2} , \tag{53}$$

then

$$O_f = 2O_2^0 Z \tag{54}$$

$$S_f = O_2^0 \frac{k_{6a}}{k_5} Z^2 . \tag{55}$$

Quenching by $O(^3P)$

Having determined k_7 (as a function of xenon pressure) and $k_5 = 1.5 \times 10^{-10}$ as well as $X_o = 4.8 \times 10^{+15} \text{ cm}^{-3}$ per atmosphere, we can proceed to calculate the absolute concentration of $O(^3P)$ and thereby determine the rate coefficients for the reactions in which it participates. Specifically, it was mentioned above that the dominant loss of $O(^1S)$ (and indirectly XeO) was expected to be through quenching by $O(^3P)$. Recent

work by Slanger (Sl75) has confirmed the previous value of rate coefficient of about $8 \times 10^{-12} \text{ cm}^3/\text{sec}$ found by Felder and Young (FY72, see also OL73). To isolate this quenching reaction in our XeO decay data we must first subtract the radiative decay component ($4 \times 10^{-15} [\text{Xe}]$). The result is displayed in Figure 23. The quenching rate coefficient obtained from these data is $4.5 \pm 0.5 \times 10^{-11}$. It is not clear whether this discrepancy originates from our absolute calibration or from some other cause. In any case, the straight-line dependence is obvious and constitutes strong support for our kinetic picture.

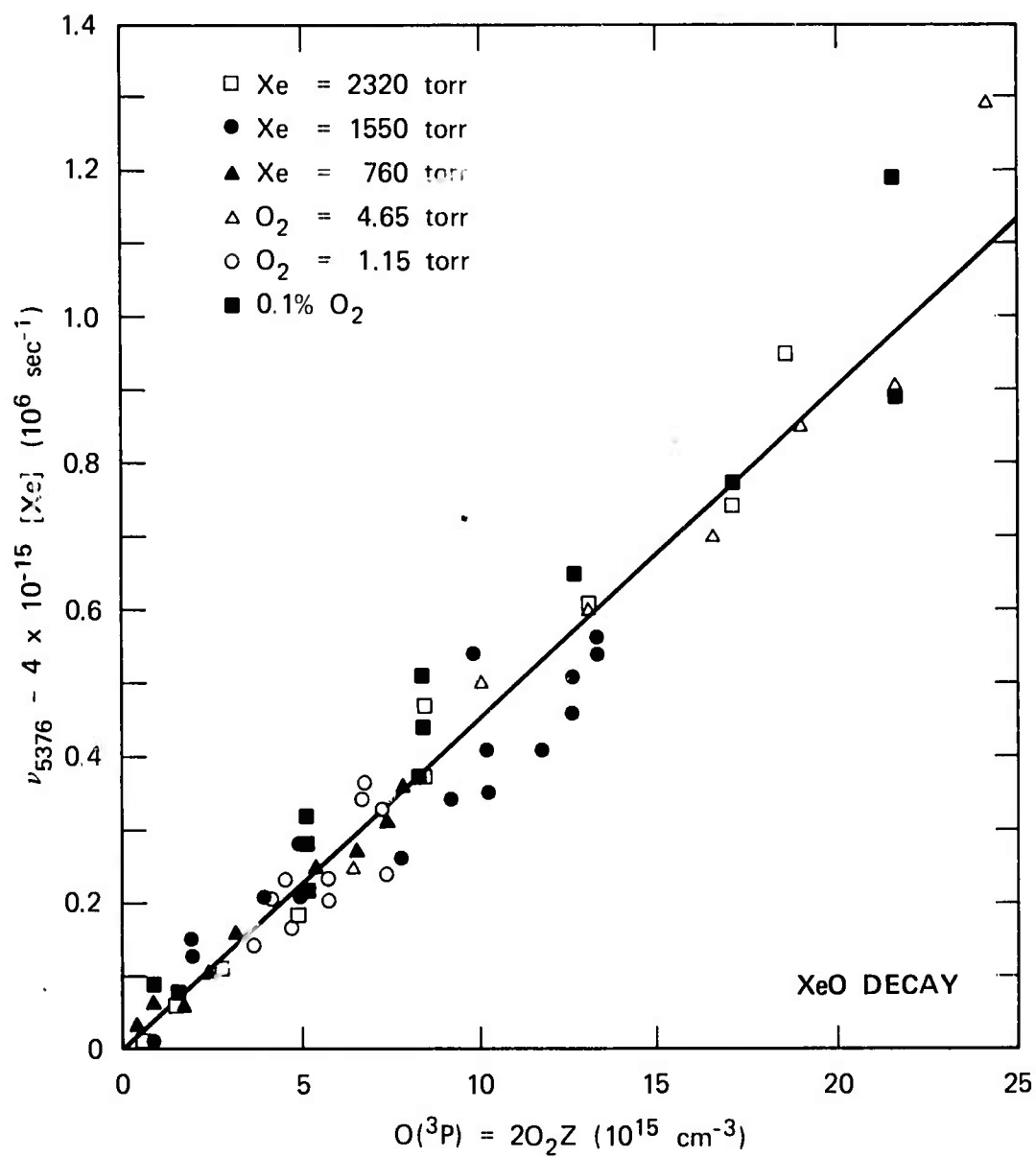
The rate of quenching of Xe_2^* by $\text{O}(^3\text{P})$ is vitally important to the hoped-for efficient operation of the XeO laser. As referred to previously, the low O_2 quenching of Xe_2^* shown in figure 16 was expected to be due to $\text{O}(^3\text{P})$. At low O_2 a large fraction of it is dissociated. The $\text{O}(^3\text{P})$ then competes effectively for the remaining Xe_2^* excimers. As the O_2 pressure is increased, a relatively smaller fraction is dissociated and O_2 becomes the dominant quencher. The expression for the final frequency of Xe_2^* reads

$$\nu_{1720} = \frac{1}{[\text{Xe}_2^*]} \frac{d}{dt} [\text{Xe}_2^*] = -k_7 - k_5 \text{O}_2 - k_6 \text{O}(^3\text{P}) \quad (56)$$

If the $\text{O}(^1\text{S})$ concentration is low, we may write this as

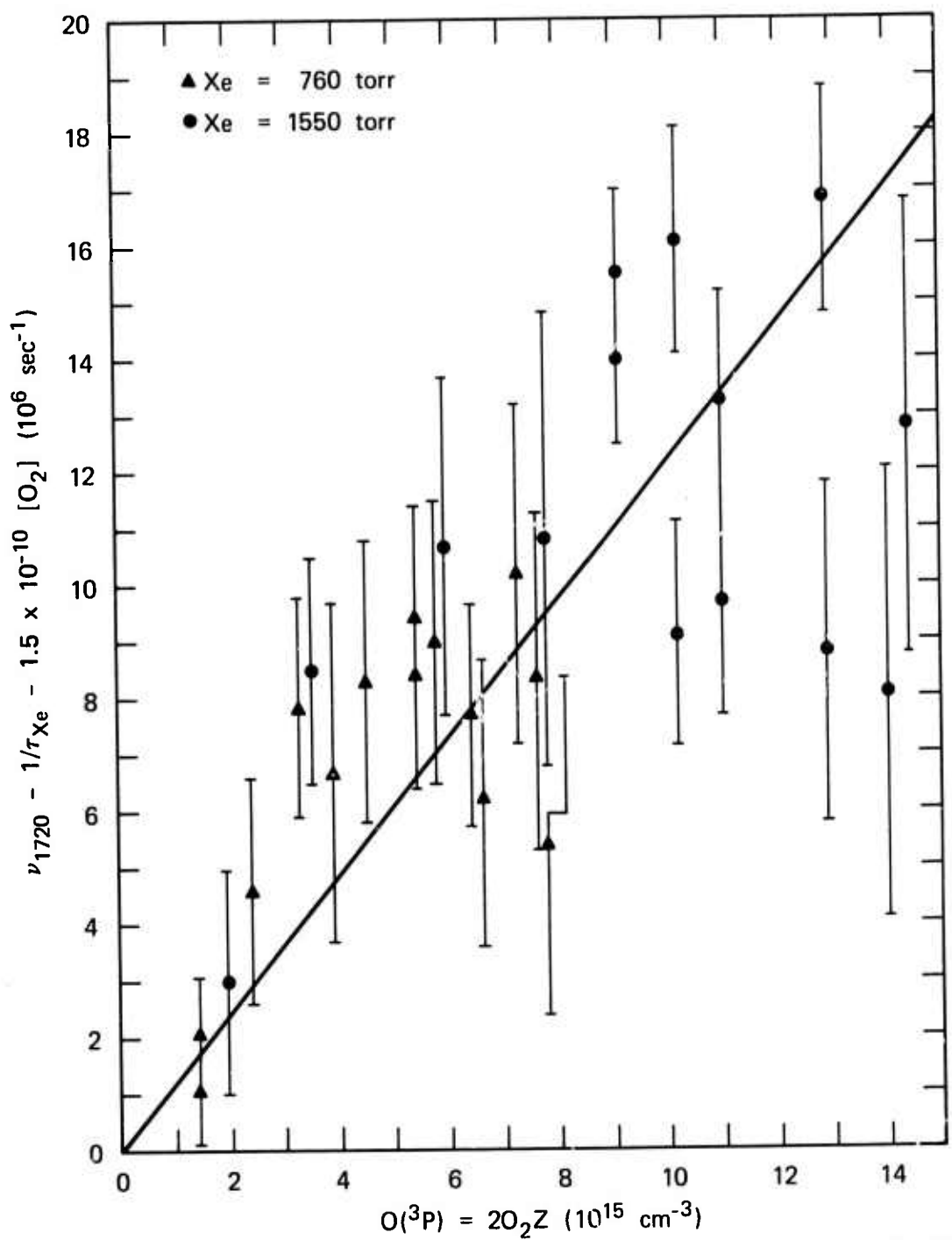
$$\nu_{1720} = -k_7 - k_5 \text{O}_2 - \left(k_6 - \frac{k_5}{2}\right) \text{O}(^3\text{P}). \quad (57)$$

Using our knowledge of k_7 (Fig. 14) and $k_5 = 1.5 \times 10^{-10}$ we may isolate the quenching due to $\text{O}(^3\text{P})$. From equations 53 and 54 we may calculate the concentration of $\text{O}(^3\text{P})$ as used in the previous graph (fig. 23). Figure 24 shows a plot of $\nu_{1720} - k_7 - k_5 \text{O}_2$ versus $\text{O}(^3\text{P})$. The data



SA-1925-102

FIGURE 23 QUENCHING OF O(¹S), AND INDIRECTLY XeO, BY O(³P)



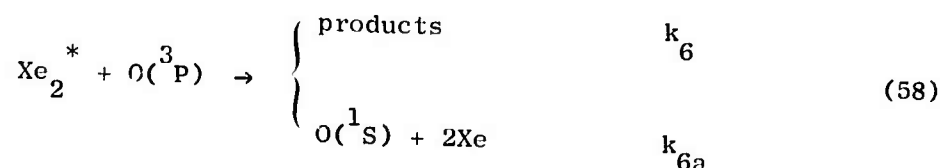
SA-1925-105

FIGURE 24 QUENCHING OF Xe_2^* BY $\text{O(}^3\text{P)}$

have become very noisy after subtraction of the dominant quenching by O_2 . Nevertheless it is possible to extract a slope, and hence a value for $k_6 - \frac{1}{2}k_5$. This yields $k_6 = 1.3 \pm .4 \times 10^{-9} \text{ cm}^3/\text{sec}$. This value is rather larger than the 5.7×10^{-10} expected from the ionic model above but once again one must remember the difficulties in the absolute calibration from which the $O(^3P)$ density was calculated.

Production of $O(^1S)$

The operating efficiency of a xenon/oxygen laser depends fundamentally on the branching ratio in the reaction

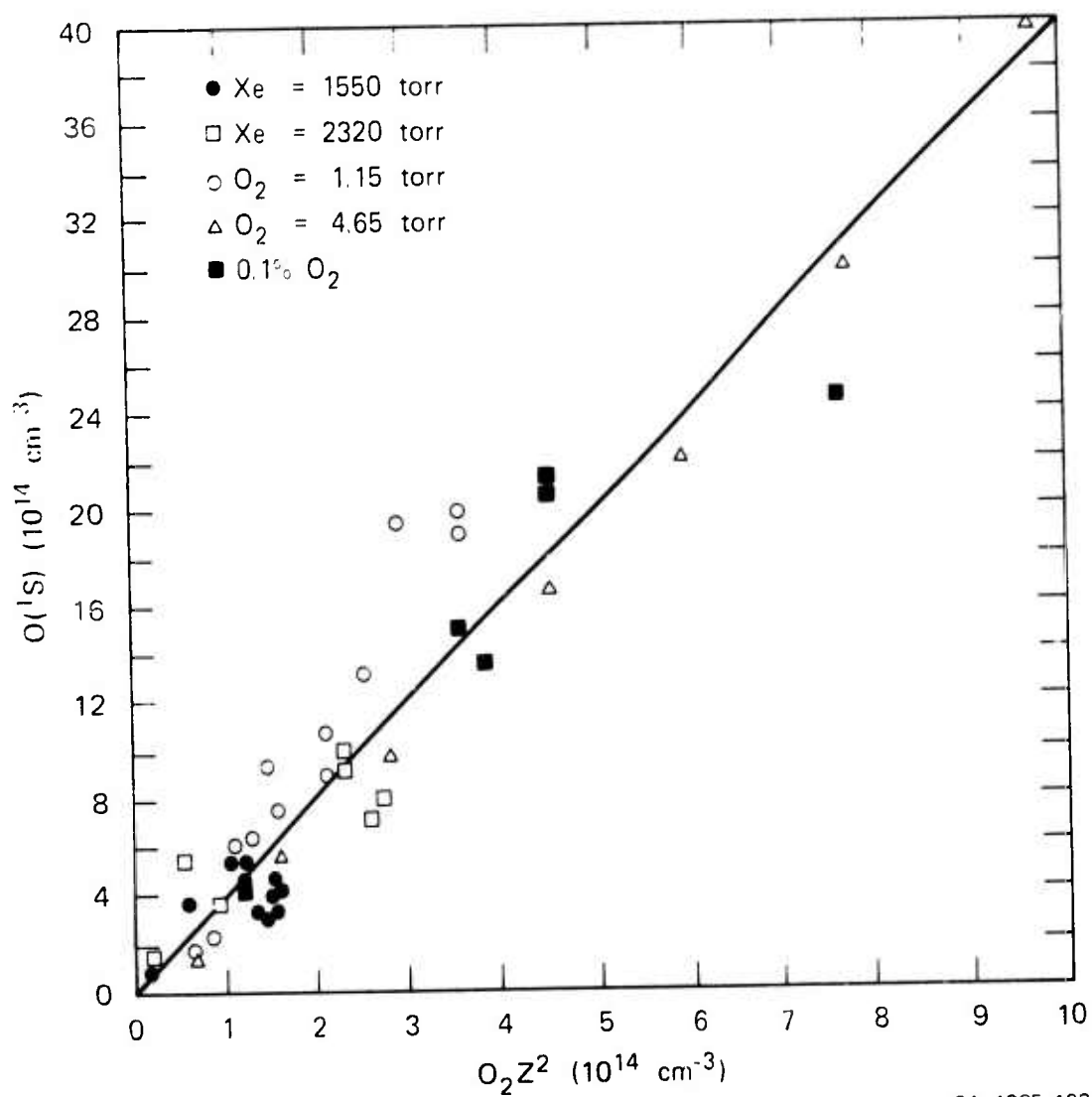


At the highest xenon pressures we have used (5450 torr), over $4 \times 10^{15} O(^1S)/\text{cm}^3$ were produced at a number efficiency of almost 12%.

Obviously, the excitation processes are relatively efficient.

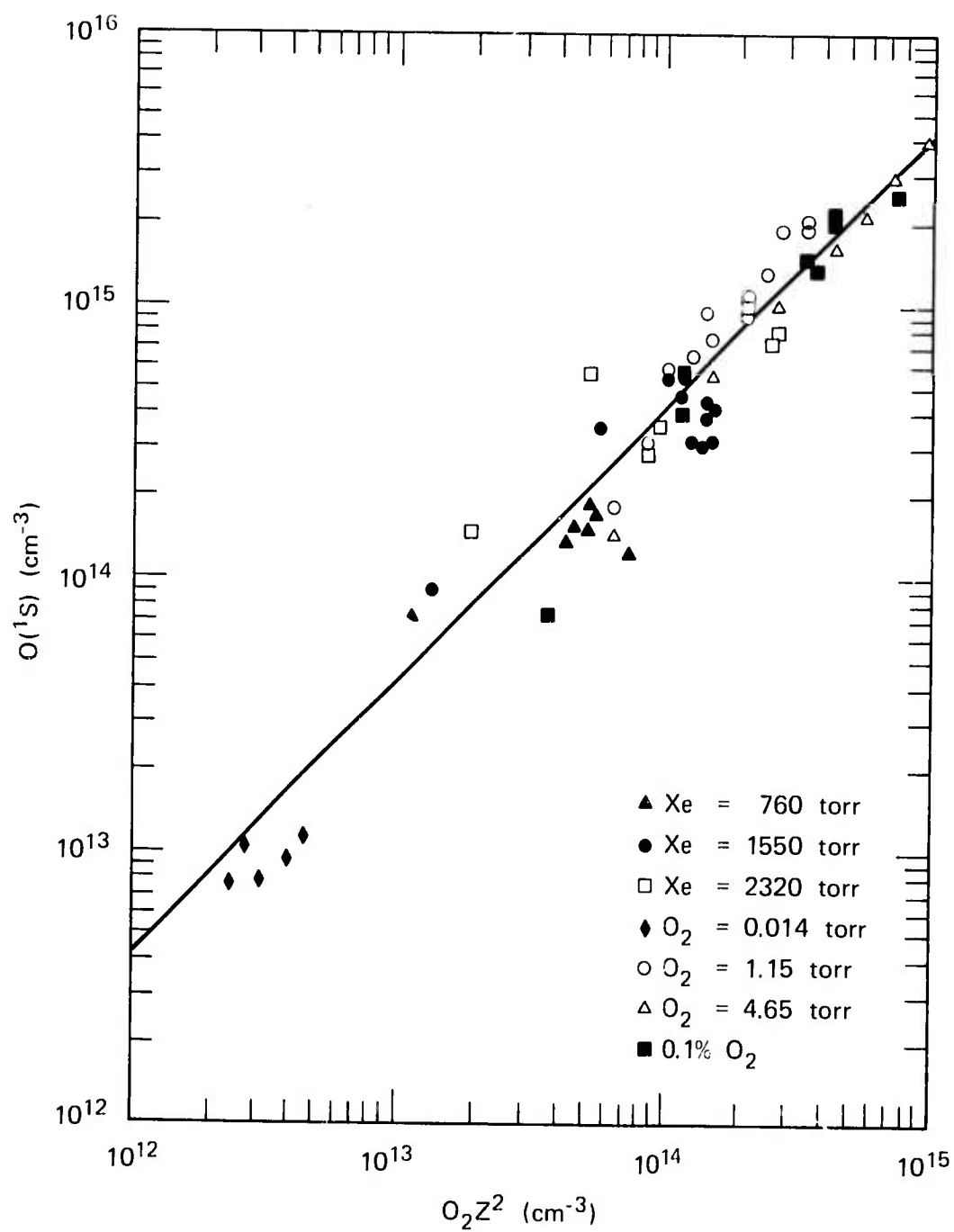
Based on our solution of the kinetic equations above (53-55), we find that a graph of the $O(^1S)$ observed versus $O_2^{O_2^2}$ should give the quantity k_{6a}/k_5 as its slope. Figures 25 and 26 show such graphs. The linear relationship is apparent. The value of the slope is not precise but yields $k_{6a} = 6 \pm 2 \times 10^{-10}$. This value is in remarkably good agreement with the 5.7×10^{-10} estimated from the ionic mechanism above. The discrepancy between k_6 , k_{6a} , and the calculated rate is not yet understood.

The various important reactions and their rate coefficients are summarized in Table V.



SA-1925-103

FIGURE 25 LINEAR PLOT OF O(1S) VERSUS O₂Z²



SA-1925-104

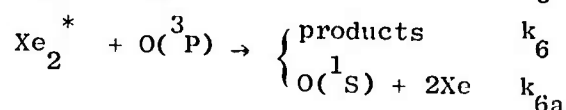
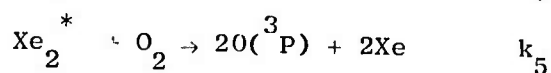
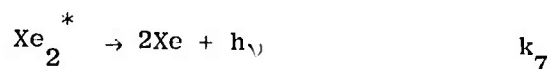
FIGURE 26 LOGARITHMIC PLOT OF $O(1S)$ VERSUS O_2Z^2

Table V
REACTIONS IN XENON/OXYGEN MIXTURES

Reaction	Rate Coefficient (cm ³ /sec etc.)	Literature Value	Reference
$\text{Xe}^* + \text{O}_2 \rightarrow \text{Products}$	--	2.2×10^{-10}	VS74
$\text{Xe}^* + \text{O}({}^3\text{P}) \rightarrow \text{Products}$	--	--	--
$\text{Xe}_2^* + \text{O}_2 \rightarrow 2\text{O}({}^3\text{P})$	$k_5 = 1.5 \times 10^{-10}$	--	--
$\text{Xe}_2^* + \text{O}({}^3\text{P}) \rightarrow \text{Products}$	$k_6 = 1.3 \pm 0.4 \times 10^{-9}$	--	--
$\text{Xe}_2^* + \text{O}({}^3\text{P}) \rightarrow \text{O}({}^1\text{S})$	$k_{6a} = 6 \pm 2 \times 10^{-10}$	--	--
$\text{Xe}_2^* \rightarrow 2\text{Xe} + h\nu$	$k_7 = \text{variable to } 6 \times 10^7$		LEH73
$\text{O}({}^1\text{D}) + \text{Xe} \rightarrow \text{O}({}^3\text{P}) + \text{Xe}$	--	$1.0 \pm 0.4 \times 10^{-10}$	DH70
$\text{Xe} + \text{O}({}^1\text{S}) \rightarrow h\nu$	$k_R = 4.0 \pm 0.5 \times 10^{-15}$	$3.7 \pm .6 \times 10^{-15}$	AW74
$\text{XeO}(2^1\Sigma^+) \rightarrow h\nu$	$k_2 = 7 \times 10^6$	7×10^6	AW74
$\text{O}({}^1\text{S}) + \text{O}({}^3\text{P}) \rightarrow \text{Products}$	$k_3 = 4.5 \pm 0.5 \times 10^{-11}$	8×10^{-12}	SJ75, FY72
$\text{O}({}^1\text{S}) + \text{O}_2 \rightarrow \text{Products}$	--	2.1×10^{-13}	SWB72
$\text{O}({}^1\text{S}) + \text{O}_3 \rightarrow \text{Products}$	--	$5.8 \pm 1 \times 10^{-10}$	IGSW71
$\text{O} + \text{O} + \text{Xe} \rightarrow \text{O}_2 + \text{Xe}$	$2.4 \pm .5 \times 10^{-33}$	} estimated from Jo68	
$\text{O} + \text{O}_2 + \text{Xe} \rightarrow \text{O}_3 + \text{Xe}$	$5.1 \pm 1 \times 10^{-34}$		
$\text{O} + \text{O}_3 \rightarrow 2\text{O}_2$	6.8×10^{-15}		

LASER OPERATION

The efficient operation of an XeO laser in e-beam excited xenon/oxygen mixtures depends on choosing the pressure and excitation conditions to obtain the optimum competition between the reactions that destroy Xe_2^* and create $\text{O}(^1\text{S})$



Enough O_2 must be provided so that most of the energy is transferred and is not lost by radiation. In addition the $\text{O}(^3\text{P})$ produced by dissociation must compete effectively with the residual O_2 for whatever Xe_2^* remains. Hence we conclude that the concentration of O_2 should not greatly exceed that of the Xe_2^* produced by the electron beam.

The kinetics of formation of $\text{O}(^1\text{S})$ and XeO occur on a 10-100 nsec time scale. In the absence of a laser field, the decay is on a 1-10 μsec time scale. Thus each $\text{O}(^1\text{S})$ produced is present at the peak in the population. Further, the rapid equilibration of $\text{O}(^1\text{S})$ with XeO means that we may refer to the production efficiencies of these two species interchangeably. We define the peak population efficiency or peak number efficiency through

$$\text{no. eff} \equiv \frac{\text{peak } [\text{O}(^1\text{S})]}{\text{total } [\text{Xe}_2^*]} \quad (59)$$

In the absence of bottlenecking, the overall laser efficiency may be calculated [as in our previous report (HGHML74)], using the formula

$$\begin{aligned} \text{laser eff} = & (\text{rare gas pumping eff}) \times (\text{quantum eff}) \\ & \times (\text{XeO}^* \text{ no. eff}) \end{aligned} \quad (60)$$

We use 50% as the efficiency with which the e-beam pump energy can be converted into xenon excimers. The quantum efficiency is just the ratio of the energy of the XeO photon (at 5376 or 3080 Å) to the 7.2 eV energy of the xenon excimer.

To estimate the maximum efficiency obtainable, we note that in the two-step dissociation and excitation mechanism, at best three Xe_2^* excimers could produce two $\text{O}(^1\text{S})$ excited atoms. This would suggest a maximum number efficiency of 67%. The inequality of k_{6a} and k_6 implies that the observed maximum number efficiency will be somewhat less. Under these assumed conditions of high energy transfer efficiency, the approximations made above in equation 48 break down, so that the approximate solutions (53-55) are no longer valid.

Specifically, if almost all the oxygen is dissociated and excited we find that

$$k_5 y > 1 \text{ and } k_{6a} y > 1 \quad (61)$$

where the effective time-variable y is defined in equation 27, and hence

$$S \approx \frac{2\text{O}_2^0}{k_{6a} - k_5} [k_{6a} - k_5] = 2\text{O}_2^0 \quad (62)$$

Further, the fact that few of the Xe_2^* excimers succeed in radiating means that

$$k_7 y \ll X_0 \quad (63)$$

and hence

$$X_o \approx \frac{k_6}{k_{6a}} S + O_2^o \approx \left[\frac{k_6}{k_{6a}} + \frac{1}{2} \right] S \quad (64)$$

Finally the asymptotic number efficiency for XeO^* becomes

$$\frac{S}{X_o} \approx \frac{1}{k_6/k_{6a} + \frac{1}{2}} \approx 38\% \quad (65)$$

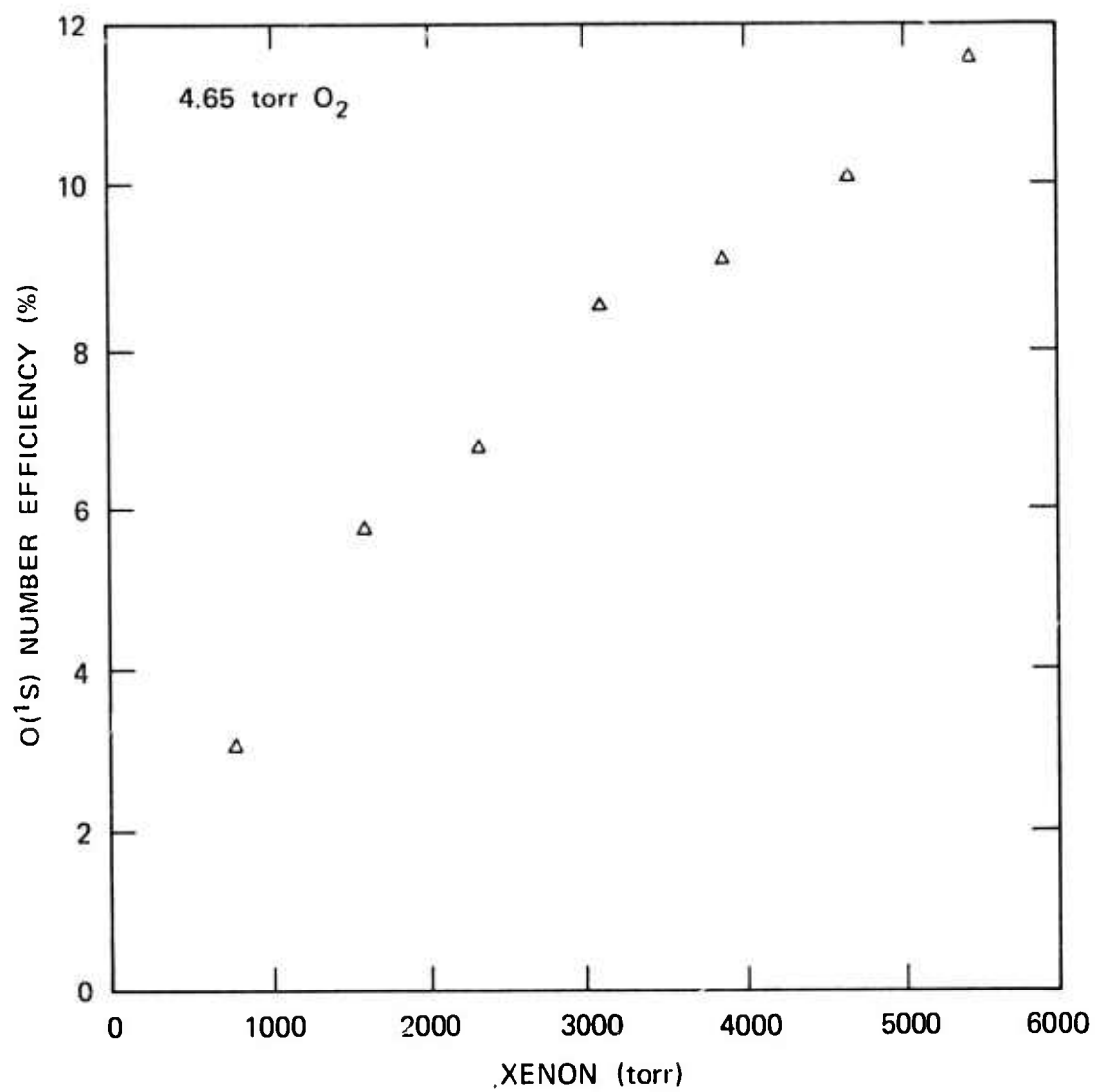
The overall laser efficiencies then become

$$\text{laser eff at } 5326 \text{ \AA} \approx (50\%) \times \left(\frac{1725}{5376} \right) \times (38\%) \approx 6\%$$

$$\text{laser eff at } 3080 \text{ \AA} \approx (50\%) \times \left(\frac{1725}{3080} \right) \times (38\%) \approx 11\%$$

To provide some further credibility to these rather large efficiencies we present in figure 27 a plot of the $O(^1S)$ number efficiency versus xenon pressure observed in our laboratory at an oxygen pressure of 4.65 torr. Even under these medium pressure, low excitation density conditions, a number efficiency of almost 12% was obtained. This corresponds to a laser efficiency of 1.9% at 5376 Å and 3.3% at 3080 Å. For comparison, Power et al. (PMR74b) have recently claimed an energy storage of 2% on the green-band transition of KrO.

For most lasers, bottlenecking becomes a serious limiting factor. This is not expected to be the case for the XeO laser. The laser action observed by Powell et al. (PMR74b) in the green bands of XeO was on the $0 \rightarrow 4$, $0 \rightarrow 5$ and $0 \rightarrow 6$ vibrational transitions from $2^1\Sigma^+$ to $1^1\Sigma^+$. One could anticipate that at the high xenon pressures to be used, vibrational relaxation in the lower state should be extremely rapid. Accumulation of a large population of $O(^1D)$ should also not be a



SA-1925-108

FIGURE 27 O(1s) NUMBER EFFICIENCY VERSUS XENON PRESSURE

problem. The quenching to $O(^3P)$ by xenon is rapid (see Table V and DH70) and is mediated by the curve crossing between the $1^1\Sigma^+$ and $1^3\Sigma^-$ shown in figure 10. The absence of a bottlenecking problem is even more apparent in the 3080 continuum band of XeO, which terminates on the repulsive $1^3\Pi$ potential curve.

Some further comments are appropriate concerning the optimum conditions for a XeO laser. The low binding energy of the upper laser level, XeO ($2^1\Sigma^+$) means that at room temperature with a reasonable xenon pressure, most of the excited oxygen exists as free $O(^1S)$. For a long pulse or cw laser operation this may be satisfactory, since the population removed by stimulated emission will be rapidly replaced by three-body association. For short-pulse high-energy operation it will be desirable to push the equilibrium from $O(^1S) + Xe$ to XeO. Since a xenon pressure of greater than 70 atmospheres would be necessary at room temperature, it is apparent that low-temperature high-pressure xenon or an obvious extension, liquid xenon, is indicated.

The observation that ozone is copiously produced by repeated e-beam excitation of xenon/oxygen mixtures, and that the intensity of the XeO emissions is thereby increased, suggests further that liquid-xenon/ozone mixtures may yield an even more efficient XeO laser. We hope to obtain further details on the kinetics of energy transfer to ozone in the near future.

We conclude this section with a pessimistic comment concerning the possibility of long pulse operation. Powell et al (PMR74a,b) have observed that laser action does not begin until the electron beam is terminated. In the analogous Kr/O₂ and Ar/O₂ systems they have found that there is a transient absorber, which disappears with the termination of the electron pulse. This absorber appears even in pure argon and krypton, and apparently eliminates the laser gain both in the green and uv bands (PM75). The definite nature of and antidote to these absorbers must be found before long pulse laser operation will be possible.

CONCLUSIONS

The spectral emission emanating from high pressure gas mixtures of Xe + O₂ excited by energetic electron beams have been examined photographically and photometrically. The results are:

(1) The excitation energy of the electron beam, initially deposited in the xenon, is rapidly and efficiently transferred (via both the Xe^{*} metastable and the Xe₂^{*} excimer) in a two-step process. The first step dissociates the O₂. The second energy transfer collision excites the resulting oxygen atoms from O(³P) to O(¹S). The O(¹S) then radiates as XeO.

(2) From analysis of the spectral and theoretical information available we have constructed semiquantitative potential curves for the low-lying states of XeO.

(3) From the six kinetic rate coefficients we have measured, combined with others from the literature, we have constructed a preliminary kinetic model which agrees well with the experimental observations.

(4) The kinetic model predicts potential laser efficiencies of 6% at 5376⁰Å and 11% at 3080⁰Å, under conditions of very high xenon density and optimally low temperature.

REFERENCES

- Ab69 A. A. Abrahamson, Phys. Rev. 178, 76 (1969).
- ABO74 E. R. Ault, M. L. Bhaumik, and N. T. Olson, J. Quant. Elec. QE-10, 624 (1974).
- AW74 R. Atkinson and K. H. Welge, "Collisionally Induced Emission of O(¹S) with He, Ne, Ar, Kr and Xe", preprint to be submitted (1974). We would like to thank R. Atkinson for allowing us to see this preprint prior to its submission.
- BHK73 D. J. Bradley, M.H.R. Hutchinson, and H. Koetser, Optics Comm. 7, 187 (1973).
- CCT61 C. D. Cooper, G. C. Cobb, and E. L. Tolnas, J. Mol. Spec. 7, 223 (1961).
- Co? C. D. Cooper, "The Visible and Near Infrared Spectra of XeO and KrO", preprint or fragment of a report (year unknown) obtained from H. P. Broida. The text is essentially the same as CCT61 but contains additional tables of rotational lines.
- CoC74 F. Collier and C. Collet, Bull. Am. Phys. Soc. 19, 156 (1974).
- CoW72 A. Corney and O. M. Williams, J. Phys. B. Atom Molec. Phys. 5, 686 (1972).
- CuC74 D. L. Cunningham and K. C. Clark, J. Chem. Phys. 61, 1118 (1974).
- DH70 R. J. Donovan and D. Husain, Chem. Rev. 70, 489 (1970).
- FLR74 P. B. Forman, A. B. Lees, and P. K. Rol, "Determination of Intermolecular Potentials Between Oxygen Atoms and Plume Species, part of a report, Private Communication (1974).
- FSW70 S. V. Filseth, F. Stuhl, and K. H. Welge, J. Chem. Phys. 52, 239 (1970).
- FY72 W. Felder and R. A. Young, J. Chem. Phys. 56, 6028 (1972).

- GHNL73 R. A. Gutcheck, R. M. Hill, D. L. Huestis, H. H. Nakano, and D. C. Lorents, Bull. Am. Phys. Soc. 18, 1581 (1973).
- GJ73a J. B. Gerardo and A. W. Johnson, J. Quant. Elec. QE-9, 748 (1973).
- GJ73b J. B. Gerardo and A. W. Johnson, J. Appl. Phys. 44, 4120 (1973).
- GR73 E. V. George and C. K. Rhodes, Appl. Phys. Lett. 23, 139 (1974).
- HGHML74 R. M. Hill, R. A. Gutcheck, D. L. Huestis, D. Mukherjee, and D. C. Lorents, "Studies of E-Beam Pumped Molecular Lasers", Technical Report No. 3, SRI No. MP74-39, Contract N00014-72-C-0478, SRI Project 1925, Stanford Research Institute, Menlo Park, California, July 1974.
- HH50 R. Herman and L. Herman, J. Phys. Radium. 11, 69 (1950).
- HO70 R. F. Hampson, Jr., and H. Okabe, J. Chem. Phys. 52, 1930 (1970).
- HSR73a P. W. Hoff, J. C. Swingle and C. K. Rhodes, Optic Comm. 8 128 (1973).
- HSR73b P. W. Hoff, J. C. Swingle and C. K. Rhodes, Appl. Phys. Lett. 23, 245 (1973).
- HSRWG74 P. W. Hoff, J. C. Swingle, C. K. Rhodes, C. W. Werner and E. V. George, VIII Int. Quant. Elec. Conf. San Francisco, June 1974.
- Hu74 W. M. Hughes, private communication (1974).
- JG73 A. W. Johnson and J. B. Gerardo, J. Chem. Phys. 59, 1738 (1973).
- Jo68 H. S. Johnson, "Gas Phase Reaction Kinetics of Neutral Oxygen Species," NSRDS-NBS20 (1968).
- KANPP46 C. Kenty, J. O. Aicher, E. B. Noel, A. Poritsky, and V. Paolino, Phys. Rev. 69, 36 (1946).
- KFRE74 K. A. Koehler, L. J. Ferderber, R. L. Readhead, and P. J. Ebert, Phys. Rev. A9, 768 (1974).
- KFRE72 K. A. Koehler, L. J. Ferderber, R. L. Readhead, and P. J. Ebert, Appl. Phys. Lett. 21, 198 (1972).

- LEH73 D. C. Lorents, D. J. Eckstrom and D. L. Huestis, "Excimer Formation and Decay Processes in Rare Gases," Final Report MP 73-2, Contract N00014-72-C-0457, SRI Project 2018, Stanford Research Institute, Menlo Park, Ca., September 1973.
- LGSW71 G. London, R. Gilpin, H. I. Schiff and K. H. Welge, J. Chem. Phys. 54, 4512 (1971).
- LHGHN74 D. C. Lorents, D. L. Huestis, R. A. Gutcheck, R. M. Hill and H. H. Nakano, "Xenon Oxide--The Kinetic Mechanism", Post deadline paper at the 4th Cont. on Chem. and Molec. Lasers, St. Louis, Mo. Oct. 1974.
- LO72 D. C. Lorents and R. E. Olson, "Excimer Formation and Decay Processes in Rare Gases," Semiannual Tech. Rpt. No. 1, Cont. N000 14-72-C-0457, SRI Project 2018, Stanford Research Institute, Menlo Park, Ca., December 1972.
- MPR74 J. R. Murray, H. T. Powell, and C. K. Rhodes, Paper P8,VIII Intl. Quant. Elec. Conf., San Francisco, June 1974.
- MR73 J. R. Murray and C. K. Rhodes, Lawrence Livermore Laboratory Report UCRL-51455, September 1973.
- MuZ71 M. J. Mumma and E. C. Zipf, J. Opt. Soc. Am. 61, 83 (1971).
- NSW71 C. Nicolaides, O. Sinanoglu, and P. Westhaus, Phys. Rev. A 4, 1400 (1971).
- OL73 R. E. Olson, Chem. Phys. Lett. 19, 137 (1973).
- PM75 H. T. Powell and J. R. Murray, private communication (1975).
- PMR74a H. T. Powell, J. R. Murray, and C. K. Rhodes, Appl. Phys. Lett. 25, 730 (1974).
- PMR74b H. T. Powell, J. R. Murray, and C. K. Rhodes, Paper MA2 4th Conf. on Chem. and Molec. Lasers, St. Louis, October 1974.
- SH74 S. K. Searles and G. A. Hart, Appl. Phys. Lett. 25, 79 (1974).
- S75 T. G. Slanger, private communication (1975).

- St74 W. J. Stevens, private communication (1974).
- SWB72 T. G. Slanger, B. J. Wood, G. Black, Chem. Phys. Lett. 17, 401 (1972).
- Ti74 G. C. Tisone, J. Chem. Phys. 60, 3716 (1974).
- Ti73 G. C. Tisone, Sandia Laboratories Report, SLA-73-1092, December 1973.
- VS74 J. E. Velazco and D. W. Setser, Chem. Phys. Lett. 25, 197 (1974).
- WHD73 S. C. Wallace, R. T. Hodgson, and R. W. Dreyfus, Appl. Phys. Lett. 23, 22 (1973).
- Wi65 J. R. Wilt, thesis, Dept. of Chemistry, University of California at Los Angeles, (1965).
- WZI53 K. Watanabe, M. Zelikoff, and E.C.Y. Inn, "Absorption Coefficients of Several Atmospheric Gases", AFCRC Technical Report No. 53-23 (1953).

APPENDIX

OPTICAL EMISSIONS FROM e-BEAM EXCITED GAS MIXTURES*

by

R. A. Gutcheck, R. M. Hill, D. C. Lorents, D. L. Huestis,
M. V. McCusker, and H. H. Nakano

Molecular Physics Center, Stanford Research Institute
Menlo Park, California 94025

MP 75-12

Abstract

A high energy electron beam has been used to pump mixtures of rare gases and atmospheric gases or metal vapors. Bright optical emissions have been produced, and a table is given listing both the observed transitions and their relative intensities.

(To be published, J. Applied Physics, August 1975)

One of the most promising efforts to produce high energy lasers operating in the visible or uv portions of the spectrum makes use of electronic energy transfer in e-beam excited high pressure gas mixtures. Recent developments in e-beam technology allow capacitor-stored energy to be converted efficiently to electron energy that can be deposited in a gas. Although e-beam excitation of most gases generally produces a variety of excited neutral and ionic states, in pure high density rare gases the deposited energy is rapidly converted to a few excimer levels (lying within a narrow energy band). These levels radiate to the dissociative ground state, giving rise to the well-known rare gas vuv continuum bands. In these systems, the conversion of e-beam to electronic state energy has an efficiency of approximately 50%.^{1,2}

The kinetics of e-beam excited high density rare gases are now sufficiently well understood to permit prediction of the population densities of the atomic and dimer ions, and the neutral atomic and dimer excited states, under both cw and pulsed excitation conditions.³ Depending on which rare gas is being pumped, electron excitation energies can vary from about 7.5 eV (Xe) to 20 eV (He). These energies are sufficient to excite a range of electronic states in any other atomic or molecular species by the mechanism of collisional energy transfer. Energy transfer processes can frequently be quite specific, leading to excitation of only a few states of the receptor. Such mechanisms can be an effective method of producing electronic state inversions.

In this paper we present the results of a survey study of optical emissions from the e-beam excitation of various rare gas-additive mixtures. The dominant emissions observed are tabulated, as well as the relative intensities of the various bands originating from a particular gas combination. The survey sought to identify potential lasing systems and this is the first of a series of papers that will include detailed kinetic studies of electronic energy transfer processes in the promising candidates.

Our experimental apparatus has been described in detail elsewhere.^{4,5} Briefly, optical emissions, resulting from the pulsed electron excitation of a gas mixture under high pressure, are viewed photometrically (RCA 1P28 and 7102 PMT) and photographically (polaroid type 57 film). A Febetron 706 (Hewlett-Packard) provides a 3-nsec 6000 amp pulse of 600 keV electrons that enters one of several target cells, some of which can be heated. A high vacuum gas handling system is connected to the stainless steel cells, and both ultra-high purity and research grade gases are used. Typical pressures were from two to four atmospheres of rare gas plus 0.1 to 5% of the additive gas. The observable spectral range extends from 1200 Å to 11,000 Å. The qualitative intensity estimates of the emissions are listed as observed, and do not account for the collisional deactivation or the absolute transition probabilities of the emitting state. The data obtained from microdensitometer traces of the photographic film did agree well with the peak intensities of the decay curves as recorded by the photomultiplier tubes. In addition to the survey results

listed here, we have examined in more detail both the temporal and spectral characteristics of some of the mixtures (e.g., Ar + N₂ + NO, Xe + O₂, and Xe + Hg); these results, including accurate number density determinations and a kinetic analysis of the relevant reactions, will appear in future papers.

The table lists the most significant emissions, with each column representing a different major gas constituent. The rare gas excimer radiation, which we observed in some cases, is not listed in the table. Column 1 contains those mixtures in which argon is the major gas present. In some cases residual gases in the Ar and N₂ gas bottles gave low intensity molecular bands, but these have not been listed. The brightest emissions are the 2+ and 1+ systems of N₂ in (Ar + N₂) mixtures, the C₂ Swan system in (Ar + CO) mixes, and the γ bands of NO. In the (Ar + CO) mixtures, we observe emissions emanating from both the v'=6 and v'=0 vibrational levels of the upper state of the Swan bands. The ratio of the peak intensity of the (6,5) emission to that of the (0,0) emission is about five at 760 torr, and decreases with increasing pressure to one at 6400 torr.

Since N₂(A³ Σ_u^+) has a very small transition probability, nitric oxide was added to the Ar + N₂ mixture to monitor the population of the N₂(A). This is because the reaction of N₂(A) with NO gives rise to the NO γ bands,^{6,7} which are more easily observed. In other cases, as listed in the fourth column, N₂(A) has been used as an intermediate energy storage level between the rare gas excitation (N₂ being 1% to 5% of the total) and a third

gas or vapor that is added, in order to observe energy transfer from $N_2(A)$. For example, mixtures of argon (2 atmospheres) and metal vapors (at a few torr) yield transitions from highly excited metal atom levels following the febetron pulse; this implies direct energy transfer from the argon metastables. When 5% N_2 is added to the mix, most of the emissions arise from much lower excited levels of the metal atom, which suggests that the predominant energy transfer occurs from the Ar to the N_2 and finally from the metastable $N_2(A)$ state to the metal.

The third column has xenon as the majority gas. The effects of the major impurity present in Xe (O_2 , which produces XeO bands), was minimized by flowing the Xe through a hot copper furnace. The table does not include these impurity emissions, but only those XeO bands due to actual dissociation of an additive gas. We found that any mixture with a minor constituent containing oxygen produces XeO emissions, except for CO, whose dissociation limit is too high.

The brightest features are the nitric oxide γ bands ($Xe + N_2 + NO$), the XeO bands ($Xe + CO_2$ and $Xe + N_2O$) and the XeHg excimer emissions from heated ($Xe + Hg$) mixtures. The γ band emissions resulting from NO reacting with $N_2(A)$ are brighter in $Xe + N_2 + NO$ than in $Ar + N_2 + NO$ for the case of identical partial pressures of N_2 and NO. This is probably due to the greater energy deposition that occurs when Xe is the absorber. The $(Xe-Ar)^+$ band at 3300 \AA has been identified by Tanaka⁸ in high pressure ($Xe + Ar$) mixtures.

Because of the lower energy of Xe^* and Xe_2^* , no N_2 $2+$ emission is produced by energy transfer. We did not see the upper $\text{N}_2(\text{B}^3\Pi_u)$ vibrational transitions ($v'=5$) as observed by Nguyen et al.⁹ This is due to two effects that occur at higher pressures: the preference of xenon metastables to form excimers over the transferring of their energy to the N_2 triplet states, and the vibrational quenching of the upper $\text{N}_2(\text{B})$ levels before they can radiate.

The second column contains emissions in which Kr was the major gas. Our emphasis has been on energy transfer in the heavier gases (Ar, Kr, or Xe). This is because of the much lower energy deposition that occurs in neon and helium, and because the metastable and excimer levels of He and Ne are high enough to cause Penning ionization or dissociation of most additives. In Kr mixtures, the brightest emissions seem to be the KrO bands (similar to the Xe + CO_2 case), the γ bands in Kr + NO, and the C_2 bands in Kr + CO. As in the case of Xe, we see little emission from Kr + N_2 .

The orientation of this survey is to investigate various gas mixtures as possible laser candidates. We have made detailed studies of the kinetics of the Ar + N_2 ,^{4,5,10} and Xe + O_2 mixtures,¹¹ both of which have demonstrated laser action;^{12,13} Xe + Hg is currently being analyzed in the same manner. Since the survey is part of a more elaborate and detailed investigation that involves the development of kinetics describing the energy flow between the gases, the results given in this paper should be viewed as the first step in providing basic knowledge that can later be used to optimize the efficiency and performance of lasing systems.

References

*This research was supported by the Advanced Research Projects Agency of the Department of Defense and was monitored by ONR under Contract No. N00014-72-C-0478

1. D. C. Lorents and R. E. Olson, "Excimer Formation and Decay Processes in Rare Gases," Semiannual Technical Report No. 1, SRI Project 2018, Contract N00014-72-C-0457, Stanford Research Institute, Menlo Park, California, December 1972.
2. E. E. Huber, D. A. Emmons, and R. M. Lerner, Opt. Comm. 11, 155 (1974).
3. C. W. Werner, E. V. George, P. W. Hoff, and C. K. Rhodes, App. Phys. Lett. 25, 235 (1974); D. C. Lorents, D. J. Eckstrom, and D. Huestis, "Excimer Formation and Decay Processes in Rare Gases," Final Report, MP 73-2, SRI Project 2018, Contract N00014-72-C-0457, Stanford Research Institute, Menlo Park, California, September 1973.
4. R. M. Hill, R. A. Gutcheck, D. L. Huestis, D. Mukherjee, and D. C. Lorents, "Studies of e-Beam Pumped Molecular Lasers," Technical Report No. 3, MP 74-39, SRI Project 1925, Contract N00014-72-C-0478, Stanford Research Institute, Menlo Park, California, July 1974.
5. R. A. Gutcheck, R. M. Hill, D. L. Huestis, D. Mukherjee, and D. C. Lorents, "Optical Emissions from e-Beam Excited Gas Mixtures. II. Ar + N₂," (in preparation).
6. R. A. Young, G. Black, and T. G. Slanger, J. Chem. Phys. 50, 303 (1969).
7. A. B. Callear and P. M. Wood, Trans. Faraday Soc. 67, 272 (1971).
8. Y. Tanaka, K. Yoshino, and D. Freeman, private communication (1974).
9. T. D. Nguyen, N. Sadeghi, and J. C. Pebay-Peyroula, Chem. Phys. Lett 29, 242 (1974).
10. D. J. Eckstrom, R. A. Gutcheck, R. M. Hill, D. Huestis, and D. C. Lorents, "Studies of e-Beam Pumped Molecular Lasers," Semiannual Technical Report No. 2, MP 73-1, SRI Project 1925, Contract N00014-72-C-0478, Stanford Research Institute, Menlo Park, California, July 1973.
11. R. M. Hill, D. J. Eckstrom, R. A. Gutcheck, D. L. Huestis, D. C. Lorents, D. Mukherjee, and H. H. Nakano, VIII International Quantum Electronics Conference, San Francisco, June 1974.

12. N. G. Basov, V. A. Danilychev, V. A. Dolgikh, O. M. Kerimov, A. N. Dobanov, A. F. Suchkov, JETP Letters 20, 53 (1974); L. Y. Nelson, G. J. Mullaney, and S. R. Byron, Appl. Phys. Lett. 22, 79 (1973); S. K. Searles and G. A. Hart, Appl. Phys. Lett. 25, 79 (1974); E. R. Ault, M. L. Bhaumik, and N. T. Olson, J. Quant. Elect. QE-10, 624, (1974); E. L. Patterson, J. B. Gerardo, and A. W. Johnson, Appl. Phys. Lett. 21, 293 (1972); R. W. Dreyfus and R. T. Hodgson, Appl. Phys. Lett. 20, 195 (1972); R. T. Hodgson, Phys. Rev. Lett. 25, 494 (1970).
13. H. T. Powell, J. R. Murray, and C. K. Rhodes, Appl. Phys. Lett. 25, 730 (1974).
14. D. C. Lorents, R. M. Hill, D. L. Huestis, R. A. Gutcheck, and H. H. Nakano, Bull. Am. Phys. Soc. 19, 1177 (1974).

SIGNIFICANT SPECTRAL EMISSIONS FROM e-BEAM EXCITED GAS MIXTURES*

Major gas Minor gas/vapor	Ar	Kr	Xe	Ar + N ₂
N ₂	N ₂ : 1+ (I) 2+ (I)	~ 4180 Å (W)	nothing significant	
O ₂		KrO: Green (B) UV (2980 Å) (W)	XeO: Green (B) UV (3080 Å) (B)	
CO	C ₂ : Swan (v'=0) (B) Hi Press (v'=6) (B) CO: 3+ (W) 4+ (W)	C ₂ : Swan (B) Hi Press (B) KrO: Green (W)	nothing significant	C ₂ : Swan (B) Hi Press (B) N ₂ : 1+ (B) 2+ (I)
NO	NO: γ (B) β (B)	NO: γ (B) β (B) KrO: Green (W) UV (F)		NO: γ (I) β (W) N ₂ : 1+ (I) 2+ (I)
N ₂ O	NO: γ (I) β (B) N ₂ : 2+ (I)		NO: γ (W) XeO: Green (B) UV (B)	
H ₂ O	OH: ~ 3065 Å (B)			
CO ₂	nothing significant		XeO: Green (B) UV (B)	
NH ₃	NH: ~ 3250 Å (W) ~ 3350 Å (B)			
Hg	Hg: atomic lines (B)		Hg: atomic lines (B) XeHg: ~ 7 ³ S-6 ³ P (I) UV (~ 2700 Å) (B)	
Cd	Cd: atomic lines (I)			Cd: atomic lines (I)
Zn	Zn: atomic lines (I)			Zn: atomic lines (I)
Tl	Tl: atomic lines (I)			Tl: atomic lines (I)
Ar			XeAr ⁺ : ~ 3300 Å (W)	
Ar + O ₂			XeO: Green (B) UV (B) XeAr ⁺ : ~ 3300 Å (W)	
Ar + N ₂ O			XeO: Green (B) UV (B) XeAr ⁺ : ~ 3300 Å (W) NO: γ (F)	
N ₂ + NO			NO: γ (I) β (B) XeO: Green (W) UV (W)	

I: Intense W: Weak
B: Bright F: Very faint